# Submillimeter fMRI Acquisition Techniques for Detection of Laminar and Columnar Level Brain Activation

Seong Dae Yun, PhD, 1 D Fabian Küppers, PhD, 1,2,3 D and N. Jon Shah, PhD,1,3,4,5\* D

Since the first demonstration in the early 1990s, functional MRI (fMRI) has emerged as one of the most powerful, noninvasive neuroimaging tools to probe brain functions. Subsequently, fMRI techniques have advanced remarkably, enabling the acquisition of functional signals with a submillimeter voxel size. This innovation has opened the possibility of investigating subcortical neural activities with respect to the cortical depths or cortical columns. For this purpose, numerous previous works have endeavored to design suitable functional contrast mechanisms and dedicated imaging techniques. Depending on the choice of the functional contrast, functional signals can be detected with high sensitivity or with improved spatial specificity to the actual activation site, and the pertaining issues have been discussed in a number of earlier works. This review paper primarily aims to provide an overview of the subcortical fMRI techniques that allow the acquisition of functional signals with a submillimeter resolution. Here, the advantages and disadvantages of the imaging techniques will be described and compared. We also summarize supplementary imaging techniques that assist in the analysis of the subcortical brain activation for more accurate mapping with reduced geometric deformation. This review suggests that there is no single universally accepted method as the gold standard for subcortical fMRI. Instead, the functional contrast and the corresponding readout imaging technique should be carefully determined depending on the purpose of the study. Due to the technical limitations of current fMRI techniques, most subcortical fMRI studies have only targeted partial brain regions. As a future prospect, the spatiotemporal resolution of fMRI will be pushed to satisfy the community's need for a deeper understanding of whole-brain functions and the underlying connectivity in order to achieve the ultimate goal of a timeresolved and layer-specific spatial scale.

Evidence Level: 1

Technical Efficacy: Stage 1

J. MAGN. RESON. IMAGING 2024;59:747-766.

The detection of neural signals using functional MRI (fMRI) at a laminar or columnar level allows the investigation of the fundamental processing of brain functions and their linked pathways between subcortical tissues. The increasing popularity of subcortical fMRI in the community is facilitated by the advance of acquisition techniques, which is the main focus of the present review paper. Since the advent of fMRI, its use as a way to map neural activities has been demonstrated in an enormous number of functional studies. The wide availability and unique advantages of fMRI over other neuroimaging modalities, such as its

noninvasiveness or unrivaled in vivo spatiotemporal resolution, have made it one of the most attractive methods with which to probe brain function. Various fMRI techniques have been suggested, depending on the purpose of a particular study. However, one of the fundamental aims pursued by most fMRI techniques is the detection of signals arising from the actual activation sites and their depiction in the spatial representation of the brain with a high mapping fidelity. Therefore, good spatial specificity is a crucial factor in fMRI techniques aiming to successfully delineate subcortical functional signals.

View this article online at wileyonlinelibrary.com. DOI: 10.1002/jmri.28911

Received Jan 27, 2023, Accepted for publication Jul 7, 2023.

\*Address reprint requests to: N.J.S., Jülich 52425, Germany. E-mail: n.j.shah@fz-juelich.de

From the <sup>1</sup>Institute of Neuroscience and Medicine 4, INM-4, Forschungszentrum Jülich, Jülich, Germany; <sup>2</sup>RWTH Aachen University, Aachen, Germany; <sup>3</sup>Institute of Neuroscience and Medicine 11, INM-11, JARA, Forschungszentrum Jülich, Jülich, Germany; <sup>4</sup>JARA – BRAIN – Translational Medicine, Aachen, Germany; and <sup>5</sup>Department of Neurology, RWTH Aachen University, Aachen, Germany

This is an open access article under the terms of the Creative Commons Attribution-NonCommercial-NoDerivs License, which permits use and distribution in any medium, provided the original work is properly cited, the use is non-commercial and no modifications or adaptations are made.

For this purpose, one approach is to employ the functional contrasts that reflect more directly physiological responses after the brain activation. Although the blood-oxygenation-level-dependent (BOLD)<sup>1</sup> contrast offers a relatively high detection sensitivity, and has thus been widely used in numerous fMRI studies, the contrast can contain signal contribution from the draining veins, which are not locally specific to neuronal activation sites.<sup>2</sup> In response to this, non-BOLD contrasts based on changes in the cerebral blood flow (CBF), cerebral blood volume (CBV), and cerebral metabolic rate of oxygen (CMRO<sub>2</sub>) have been proposed,<sup>3–5</sup> and have been shown to have more direct relevance to metabolic changes stemming from the neural activities.<sup>2</sup>

Another methodological approach to improve the mapping specificity is to increase the spatial resolution of the imaging technique. Using a reduced voxel size can aid the more distinct sampling of brain tissue, resulting in reduced partial volume effects (PVEs) and thereby increasing spatial specificity. The reduced PVE can also lead to increased functional sensitivities as the activation signals are less affected by surrounding nonactivated regions.<sup>6</sup> The spatial resolution of fMRI has been drastically improved by virtue of hardware developments and imaging techniques. For instance, high-performance gradient systems and a large number of receiver channels in the radiofrequency (RF) coil facilitate the use of a relatively large imaging matrix size and acquisitions can be highly accelerated by fast imaging techniques (eg parallel imaging or multi-band, etc.). <sup>7,8</sup> Furthermore, developments at ultra-high fields (UHFs) offer increased signal-to-noise (SNR) and contrast-to-noise (CNR) ratios compared to lower field strengths, which ensures the robust detection of neural activities with a submillimeter voxel size for a group of subjects.9 An additional benefit of UHF imaging is that the BOLD contrast arises predominantly from capillaries and becomes more localized to surrounding tissues due to the fact that the contribution of the microvascular component becomes dominant over that of the macrovascular component. The much shorter  $T_2$  of blood water than that of tissue also yields a reduction of the intravascular contribution to the BOLD signals.<sup>6</sup> Figure 1 shows an exemplary result from visual fMRI, illustrating the effect of the improved spatial resolution on the detection of BOLD signals.

As a result of the described advances in fMRI, a number of previous studies have endeavored to acquire functional data with a submillimeter voxel size and have attempted to characterize the subcortical activation pattern. This kind of investigation can provide insight into the fundamental unit of neuronal organizations and the consequent hierarchical processing in the brain function. In addition, several early works successfully identified orientation columns or feedforward/feedback pathways to different cortical layers and columns. <sup>10–13</sup> Although the research findings have been derived from healthy volunteers, most submillimeter fMRI studies suggest the use of high spatial resolution to aid improved clinical diagnosis. For instance, the examination of frequency-specific responses in

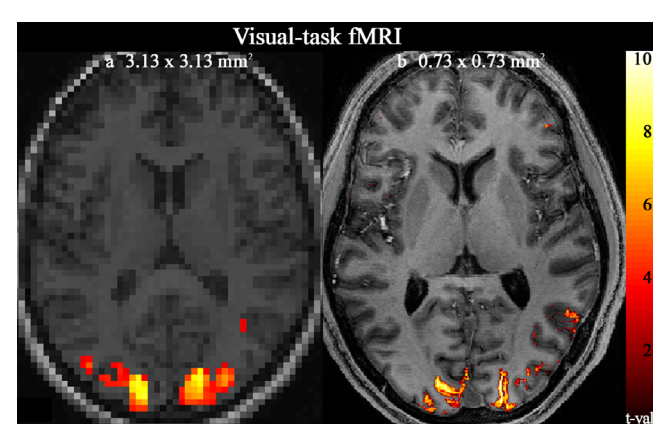


FIGURE 1: Results of visual task-fMRI obtained with (a)  $3.13 \times 3.13 \text{ mm}^2$  and (b)  $0.73 \times 0.73 \text{ mm}^2$ . Both results were obtained using the 2D GE-EPI method, and the activated voxels identified with an uncorrected *P*-value <0.001 are overlaid onto the co-registered MPRAGE scan. This figure depicts how a higher spatial resolution in fMRI exhibits improved localization of activated voxels compared with a low-resolution case.

tinnitus patients requires a substantially higher spatial resolution than that conventionally used ( $\sim$ 2 × 2 × 2 mm<sup>3</sup>) to investigate functions in subcortical auditory structures such as the medial geniculate body and inferior colliculus. <sup>14</sup>

In this paper, we mainly focus on a review of the fMRI techniques that enable the detection of brain function at a subcortical level. Here, the technical innovations and challenges of each imaging technique are described and compared. Techniques to generate functional contrast are first discussed, followed by a discussion relating to the image readout techniques used to depict said functional contrasts. We also introduce supplementary methods to overcome the limitations of current fMRI techniques for improved mapping accuracy with reduced geometric distortions.

# **fMRI Contrasts**

This chapter summarizes the measurable functional contrasts employed in fMRI. The achievable fMRI attributes depending on functional contrasts are shown in Table 1. A schematic representation of the measurable parameters and their underlying physiological tissue characteristics is depicted in Fig. 2.

# Blood-Oxygenation-Level-Dependent

The higher demand for oxygen caused by neuronal activities induces increased blood flow, resulting in the increase of the oxyhaemoglobin (Hb)/deoxyhaemoglobin (dHb) ratio. This phenomenon increases the  $T_2/T_2^*$  of blood water inside the vasculature (intravascular [IV]), which creates local field gradients (i.e. susceptibility effects) that extend to the surrounding tissues (extravascular [EV]). The consequential signal changes, relative to the rest condition, become the functional contrast. This BOLD contrast relates to the changes in other physiological parameters, such as CBV, CBF or oxygen

TABLE 1. Summary of fMRI Attributes Depending on	
Functional Contrasts	

MRI Attributes	Comparison
Functional sensitivity	BOLD > Non-BOLD
Spatial specificity	Non-BOLD > BOLD
Temporal efficiency	BOLD > Non-BOLD; Non-BOLD contrasts require an additional contrast preparation module, leading to a substantial increase of the minimum TR required (i.e. a few seconds).
Power requirement	Non-BOLD > BOLD; The tagging or inversion pulses employed in the contrast preparation module of the non-BOLD contrasts significantly increase the required power level.
Brain coverage	BOLD > Non-BOLD; The increased volumetric TR and energy level in non-BOLD contrasts may restrict the allowed brain coverage.
Invasiveness	A gas challenge is required for CMRO <sub>2</sub> .

Comparison of fMRI contrasts is given for the addressed fMRI attributes. The non-BOLD contrasts include CBF, CBV, and CMRO<sub>2</sub>. Depending on the readout (Section 'Sub-mm fMRI Techniques') and Supplementary (Section 'Supplementary Techniques for Accurate Spatial Mapping') techniques, each fMRI attribute can be more specifically determined.

metabolism.<sup>15</sup> In addition, the effects in the two BOLD signal components, IV and EV, originate not only from small vessels relating to the local neural activity, but also from large draining veins which detrimentally affect spatial specificity.<sup>6</sup>

This complex behavior of the BOLD contrast makes its quantitative analysis rather difficult. However, the venous IV contribution diminishes at a higher field strength, and the BOLD contrast becomes more specific to activated tissues. Previous work on rat brains has reported that venous blood has a significantly shorter  $T_2$  (9.2  $\pm$  2.3 msec) than the somatosensory cortex (38.6  $\pm$  2.1 msec) at a mean oxygen saturation level of 79.6  $\pm$  6.1%. The BOLD contrast can be acquired using various imaging techniques (see Section 'Sub-mm fMRI Techniques') without an additional contrast preparation module, which usually results in a higher temporal sampling efficiency (eg from sub to a few seconds) compared to non-BOLD contrasts.

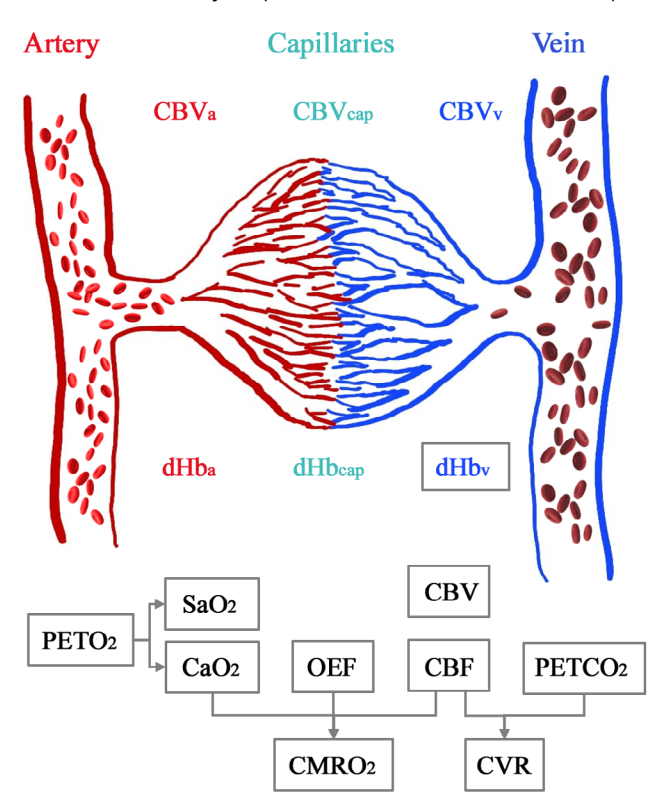


FIGURE 2: Overview of the physiological parameters that describe blood metabolism. This figure depicts fundamental parameters linked to neural activity, such as CBV in the artery, capillary and vein, as well as the dHb concentration in those regions. The described parameters in gray boxes are measurable by fMRI or other appropriate neuroimaging techniques. PETO<sub>2</sub> allows the quantification of arterial oxygen saturation (SaO<sub>2</sub>) and arterial oxygen content (CaO<sub>2</sub>). The latter quantity can be translated together with CBF and OEF to CMRO<sub>2</sub>. The measurement of CBF for end-tidal carbon dioxide (PETCO<sub>2</sub>) gives rise to the quantity of cerebrovascular reactivity (CVR).

# Cerebral Blood Flow

Neuronal activity leads to arterial dilation which ultimately entails a change in the blood supply.<sup>3</sup> The resulting contribution of blood flow and volume to the fundamental BOLD signal makes CBF an important physiological parameter that reflects microvascular density during rest as well as vascular reactivity to functional activation.<sup>15</sup> CBF was observed to show large variations over the whole cortex, while the resting CBF has the potential to indirectly reflect brain metabolism under the assumption of a homogeneous oxygen extraction fraction.<sup>17</sup> Thus, quantification of CBF offers a fundamental parameter for the characterization of neurovascular function.<sup>3,18</sup>

The measurement of this contrast is usually performed using arterial spin labeling (ASL),<sup>3,18</sup> which first labels the arterial water protons by either saturation or inversion pulses prior to their arrival in the desired imaging volume and then performs data readout after a sufficient delay to allow exchange of the labeled spins with the tissue. Here, the subtraction of the tagged image from the control image acquired

without the tagging pulse can depict the contrasts created by the changes in blood flow. An illustration of contrast generation using ASL is shown in Fig. 3a. In this way, ASL signals can represent neural activations confined in the regions where the dominant part of the labeled arterial water exchanges with tissue water in the capillaries. However, despite providing high spatial specificity, ASL suffers from a higher RF power deposition and a lower SNR than BOLD, which usually require careful optimization of the labeling scheme or imaging protocols. 18,19 Here, the required time for the contrast preparation differs depending on the labeling scheme. However, for the labeling schemes that are practically implementable in most clinical MRI systems (i.e. pulsed ASL or pseudo-continuous ASL), the preparation duration is usually around  $2 \sim 3$  s at 7 T, as demonstrated in recent subcortical fMRI studies. 18-20 Therefore, in non-BOLD fMRI, like ASL-fMRI, the volumetric TR is constituted by the time for the preparation module as well as the data sampling readout.

### Cerebral Blood Volume

During brain activation, increased CBF leads to CBV changes, the measurement of which was shown to be locally specific to parenchyma.  $^{4,21,22}$  Thus, CBV is an important biomarker for tissue viability and vascular reactivity. To derive the CBV contrasts depending on the vascular space occupancy (VASO), an imaging technique has been presented that utilizes the fact that the longitudinal relaxation times ( $T_1$ ) of tissue and blood are different. That is, following the application of an inversion pulse, the data readout is started at the time that the recovered blood signals reach the zero-crossing point. This is done to suppress blood signal

contribution to the reconstructed images. During brain activation, a further signal decrease is expected in the regions associated with the neuronal activation due to the vascular dilation effects. A resultant functional contrast image can be created by comparing images during rest and activation. The underlying concept of VASO is illustrated in Fig. 3b. In this method, the required inversion time for blood-nulling is around 1 s at 7 T.<sup>2,23</sup> However, to further correct the BOLD contamination from the resulting signals, another inversion process  $(3 \sim 4 \text{ s})$  may also be adopted as suggested in sliceselective-slab-inversion VASO.<sup>23</sup> One limitation of VASO is that it only reflects relative CBV changes, and its signal strength relies on the baseline blood volumes, which can be different with respect to the cortical depth. 18 Furthermore, compared to GE-BOLD contrasts, VASO increases RF power deposition due to the inversion preparation pulse making it challenging at ultra-high fields. Another imaging method to quantify CBV is ASL, which is capable of the simultaneous measurement of CBF and CBV.<sup>24</sup>

### Cerebral Metabolic Rate of Oxygen

As described above, the BOLD contrast relies on various elements of baseline physiology (eg CBF, CBV, CMRO<sub>2</sub>), meaning that signal changes can be affected by not only the metabolic response but also subject-dependent vascular factors, like vascular volumes or cerebrovascular reactivity.<sup>25</sup> This complication motivated the development of a BOLD calibration technique that can quantify the non-neural components and then remove them from the obtained functional signals so that a stimulation-elicited, quantitative estimation of CMRO<sub>2</sub> can be obtained.<sup>5,22,25</sup> The calibration technique

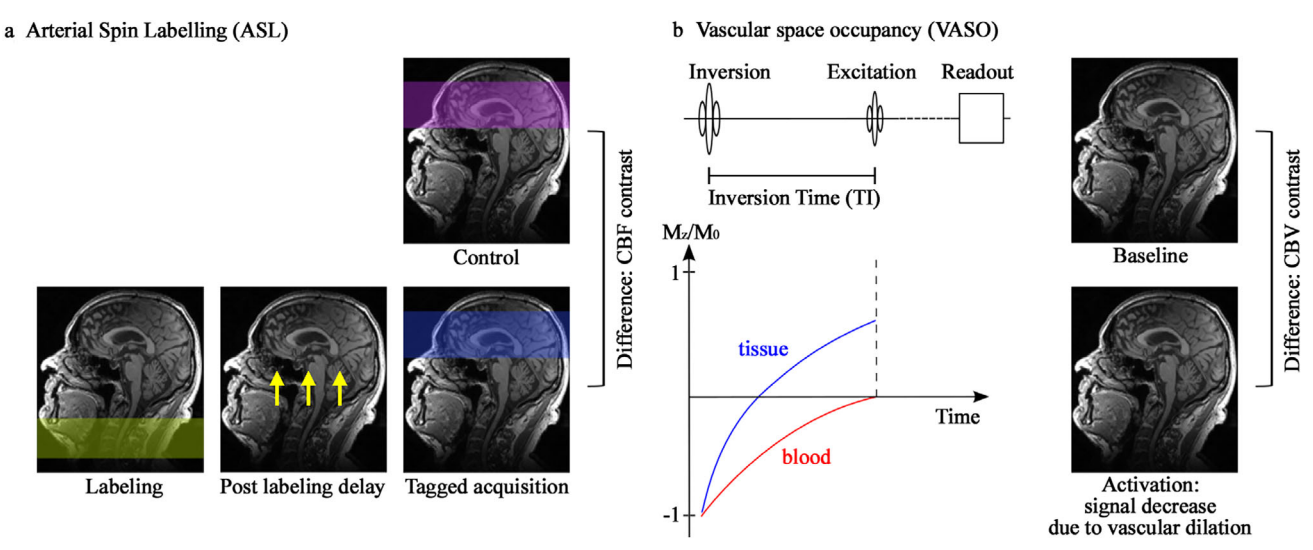


FIGURE 3: Illustration of contrast generation for fMRI by ASL and VASO. (a) The ASL technique is based on labeling the arterial water spins and a certain delay during which these spins can exchange with tissue. The resulting image is subtracted from a control image acquired without the spin labeling. The resulting information reflects blood flow contrast. (b) In the VASO technique, an inversion pulse is applied, and data readout is started at the time such that the signal from the blood water should be suppressed. During brain activation, vascular dilation leads to a further signal decrease in the activation region when compared to the resting state. This signal difference provides the CBV contrast.

Yun et al.: Layer-Specific Submillimeter fMRI Techniques

modulates the blood gas using hypercapnia, hyperoxia or a combination of both (i.e. dual-calibration). This modulation manipulates the BOLD signal amplitude and subsequently allows the estimation of the maximum BOLD signal changes (*M*). This can be expressed as follows<sup>5,25</sup>:

$$\frac{\Delta \text{BOLD}}{\text{BOLD}_0} = M \left( 1 - \left( \frac{\text{CBV}}{\text{CBV}_0} \right) \left( \frac{[\text{dHb}]}{[\text{dHb}]_0} \right)^{\beta} \right),$$

where the subscript 0, [dHb], and  $\beta$  denote the resting state, dHb-concentration in blood and a constant describing the influence of dHb on transverse relaxation, respectively.

The equation is used as a basis model for the BOLD calibration, although a further modification of this equation and a slightly different quantification procedure is required depending on the gas challenge methods; Davis et al,<sup>5</sup> Chiarelli et al,<sup>26</sup> and Generalized Calibration Models<sup>25</sup> are used for the hypercapnia, hyperoxia, and dual-calibration cases, respectively. The above equation suggests that BOLD and CBF (or CBV) measurements should be used as inputs, and in the case of CBF, its quantity can be transferred to CBV using Grubb's relation: CBV/CBV<sub>0</sub> = (CBF/CBF<sub>0</sub>)<sup>0.38</sup>. Here, a simultaneous measurement of BOLD and CBF (or CBV) is possible using the dual-echo ASL (or VASO) methods, indicating that the same contrast preparation (i.e. tagging or inversion) module is also involved in CMRO<sub>2</sub> fMRI.

# **Sub-mm fMRI Techniques**

This section describes data readout techniques that can be used to detect the functional contrasts described above. Table 2 summarizes a typical imaging parameter set from each imaging technique and the corresponding previous literature that demonstrates the detection of subcortical brain activation.

### 2D GE-EPI

For effective detection of dynamic haemodynamic responses, the imaging technique usually needs to offer a high temporal resolution. This condition is well satisfied with EPI. 49 In this scheme, the zig-zag traversal of k-space requires the gradient pulses to rapidly change, the rate of which is determined by the performance of the gradient system (eg slew rate). A higher rate allows an increased spatiotemporal resolution in EPI, which is beneficial for submillimeter-resolution fMRI. Although EPI can generate ghost artifacts as a result of the zig-zag acquisition and technical limitations (eg eddy currents), the artifacts can be effectively eliminated by means of the phase-correction (each line in a given direction is affected in a similar manner). Various EPI-based methods have been developed and of these, 2D gradient-echo (GE) EPI is the most commonly used. This is largely because of its relatively simple sequence structure (i.e. easy implementation; see

Fig. 4a) and good SNR level with relatively little concern regarding the specific absorption rate (SAR).

In the BOLD fMRI studies, GE-based methods provide a higher functional detection sensitivity than spin-echo (SE)-based methods. However, as described in above, the BOLD signals detected with the GE sequences contain the contribution not only from the local microvasculature but also from the macrovasculature, leading to the phenomenon of functional signals detected at the superficial layers being larger than those at the deeper layers.  $^{11,33,50}$  The two major mechanisms that create this superficial bias are as follows: 1) crosstalk introduced by ascending draining veins that carry the deoxygenated hemoglobin from the deep to the superficial layers (i.e. leakage effect); and 2) different physiological parameters (eg baseline CBV or  $T_2$ \*) across the cortical depth (i.e. multiplicative effect)  $^{33,41,50}$ ; a schematic illustration of this mechanism is shown in Fig. 5.

These bias effects negatively affect the spatial specificity of the activated voxels, which may have an impact on the characterization of subcortical functional profiles. To avoid this conflict, alternative imaging sequences based on SE or steady-state free precession (SSFP)<sup>51</sup> have been presented. However, in regard to the functional sensitivity, previous works have reported that, when compared to SE-EPI, GE-EPI shows 1.29 and 5.33 times higher percent signal changes in gray matter (GM) and in vessels at 7 T, respectively.<sup>52</sup> The vascular blurring in GE-BOLD can also be circumvented by means of non-BOLD fMRI techniques, such ASL or VASO. However, these latter techniques are also accompanied by reduced functional sensitivity (10%-20% for ASL and 40%-60% for VASO, compared to GE-BOLD) or a much longer volumetric TR, making the robust detection of neural activation for whole-brain challenging. 9,15,33 For this reason, GE-BOLD techniques still continue to be used in submillimeterresolution, subcortical fMRI studies, in which the effects of the large vessels are instead alleviated using the additional correction methods. 9,11,13,21,28,31

### 2D SE-EPI

The SE technique recreates spin phase coherence by using a  $180^{\circ}$  pulse following the excitation pulse (see Fig. 4b). In BOLD fMRI, this technique suppresses the static dephasing effects generated from the field inhomogeneities around large vessels. Therefore, the functional contrast components contributing to SE-BOLD (i.e.  $T_2$  contrast) are known to be the IV changes and the EV changes driven by diffusion-induced dynamic averaging of field inhomogeneities generated from dHb-containing components, which are restricted to the microvasculature. Due to the shorter  $T_2$  of venous blood at UHFs, the IV contribution to the BOLD signals becomes weaker, and the microvascular contributions from the EV BOLD effect dominate the functional contrast, which is more specific to the neuronal activation site.

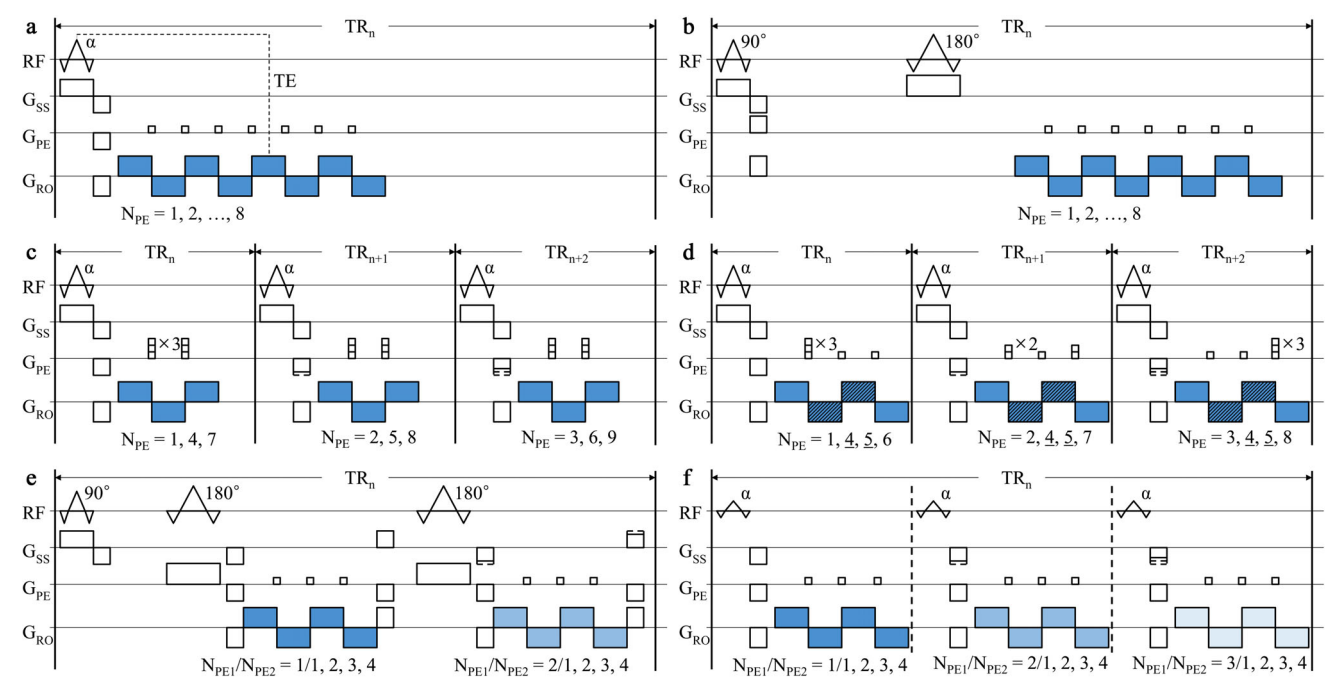


FIGURE 4: Schematic representation of the sequence diagram for the EPI-based readout techniques. (a) 2D GE-EPI, (b) 2D SE-EPI, (c) 2D three-shot EPI, (d) 2D three-shot EPIK, (e) 3D inner-volume GRASE, and (f) 3D GE-EPI. For simplicity, the following sequence components are not depicted: navigator echoes, spoiling gradient, and crusher gradients, each of which is for the elimination of N/2 ghost artifacts, remaining transversal magnetization and unwanted echoes in the SE-based methods. Here,  $TR_n$  denotes the volumetric TR, and colored (blue) gradients represent the point at which the data sampling is performed. For the 3D sequences (e and f), the data at different slice locations are presented with light blue, whereas the 2D sequences (a–d) are only depicted in the diagram for the single-slice case. In EPIK (d), the central k-space lines (i.e.  $N_{PE} = 4$  and 5), further marked with a hatched pattern, are sampled to ensure optimum SNR and CNR for every temporal scan.

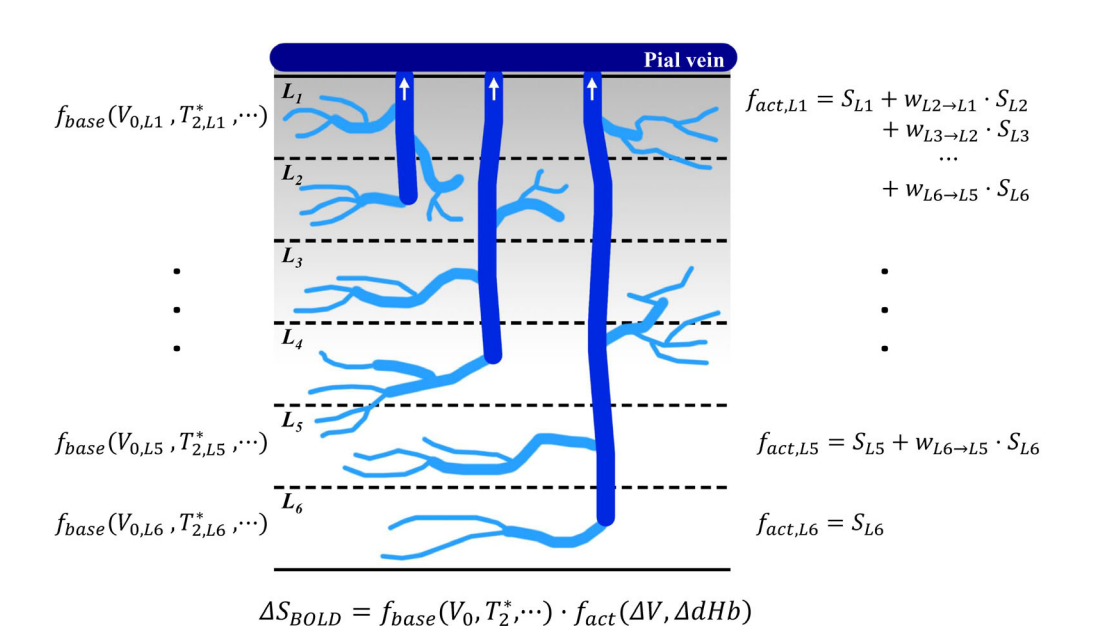


FIGURE 5: Schematic representation of the depth-dependent vascular contribution on BOLD signals. Cortical layers are denoted with  $L_n$  where n is from 1 to 6. The BOLD signal change,  $\Delta S_{BOLD}$ , can be formulated as the product of the baseline factor,  $f_{base}(V_0, T_2^*, ...)$  and the signal changes induced by the brain activation,  $f_{act}(\Delta V, \Delta dHb)$ . The signal components of the latter term further consist of contribution from the venules (local microvasculature; colored in light blue) and the draining ascending veins (macrovasculature; colored in blue). The dHb carried by the ascending veins leads to a signal contribution from the deeper layers to the upper (i.e. leakage effect), as described with the formula on the right side of the figure. The baseline factor represents the intrinsic physiological parameters such as baseline blood volume,  $V_0$  or transverse relaxation time,  $T_2^*$  at a certain layer location, which is considered as a multiplicative factor to the BOLD signal,  $\Delta S_{BOLD} = f_{base}(V_0, T_2^*, \cdots) \cdot f_{act}(\Delta V, \Delta dHb)$ .

However, implementation of SE-EPI introduces considerable  $T_2^*$  dependence as a result of the long readout length. Therefore, a restricted readout length, eg  $1.25 \times T_2^*$ , is often used in SE-EPI to avoid the significant loss of spatial specificity arising from the T<sub>2</sub>\*-induced point-spread-function (PSF) broadening.  $^{6,35}$  To achieve a purer  $T_2$  contrast, alternative readout methods, such as 3D Gradient-and-Spin-Echo (GRASE),<sup>53</sup> Echo Planar Time-resolved Imaging (EPTI),<sup>36</sup> or even line-by-line excitation-based methods,  $T_2$ -prep GE<sup>54</sup> and balanced SSFP (bSSFP)<sup>55</sup> can be used. Although the SE-BOLD method can offer improved spatial specificity compared to GE-BOLD, the disadvantages, such as the reduced BOLD sensitivity hinder the robust use of high-resolution (i.e. low SNR) SE fMRI for group studies. A further disadvantage is that the increased RF power deposition due to the 180° pulse and the underlying  $B_1$  field inhomogeneities may restrict the number of achievable imaging slices per time frame (i.e. limited brain coverage). This also requires the careful control of multiple extra-echo coherence pathways, such as stimulated echoes, which arise from the successive application of imperfect refocusing. 10

### 2D Multi-Shot EPI and EPIK

The spatial resolution of EPI can be improved with a greater number of phase-encoding lines, which directly leads to a longer readout length. In single-shot EPI, the prolonged readout duration gives rise to an increase in  $T_2$ \* blurring or geometric distortion artifacts. Therefore, SNR considerations notwith-standing, the arising issues, coupled with the long readout duration, hinder the direct use of single-shot EPI for high-resolution, whole-brain fMRI. This difficulty can be mitigated with the in-plane acceleration techniques, such as parallel imaging  $^7$  or partial Fourier techniques,  $^{56}$  which, however, introduce a substantial SNR reduction or image blurring. An alternative approach is to split the long EPI echo

train into several segments, each acquired with an individual RF excitation, i.e. multi-shot EPI (see Fig. 4c). In contrast to the aforementioned in-plane acceleration techniques, in principle, the multi-shot scheme does not lead to any additional image SNR reduction. Here, the greater the number of segments, the more the problems associated with the long readout can be reduced, which, however, comes at the cost of an increased acquisition time and a greater susceptibility to physiologically induced artifacts; Fig. 6 shows the effect of the multi-shot scheme on the reduction of geometric distortions.

Crucially, another major drawback of multi-shot EPI for fMRI is its shot-to-shot instabilities that can create intermittent ghost artifacts or increased susceptibility to subject motion and respiration-induced field changes. <sup>36,37</sup> These artifacts can corrupt the temporal stability of the fMRI time-series data, consequently affecting the detection sensitivity. Figure 7 shows the deleterious effects of the multi-shot scheme on the detection of activated voxels when compared to single-shot EPI. To make the use of multi-shot EPI for fMRI feasible, an alternative shot-reordering scheme has been presented, which acquires all the segments for each slice completely before proceeding to the next slice, namely fast low-angle excitation echo-planar technique (FLEET) or its variable flip angle progression (VFA-FLEET). <sup>37,57</sup>

Another approach to overcome the limitation of multishot EPI is to sample the central portion of *k*-space in every shot, as proposed in the EPI with Keyhole (EPIK) technique (see Fig. 4d). 9,58–64 As most information relating to natural images is confined around lower frequencies, sampling the central *k*-space ensures optimum SNR and CNR for each individual shot. 61,62 In this way, EPIK has been shown to have a higher temporal resolution and reduced geometric distortions than EPI, with a very marginal decrease in temporal SNR. 61,62 When compared to multi-shot EPI, EPIK shows more robust functional detection performance, which is

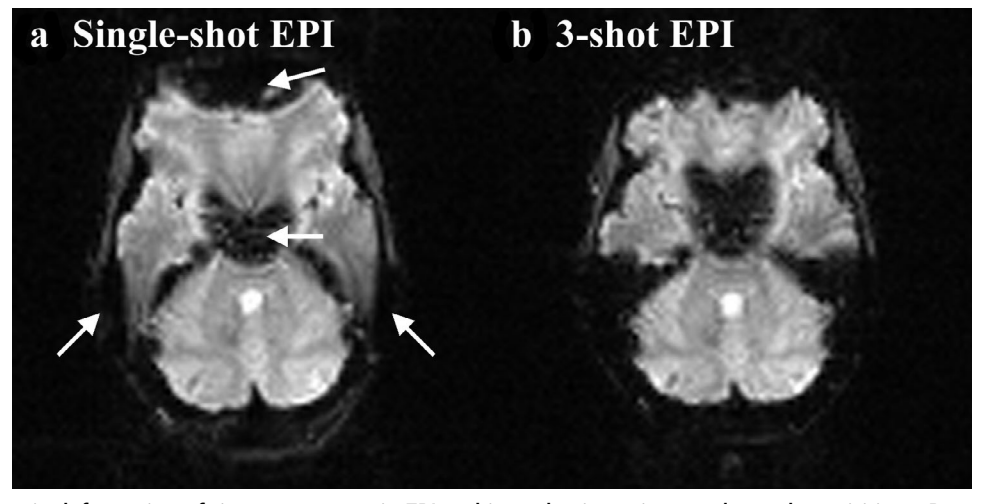


FIGURE 6: Geometric deformation of tissue structures in EPI and its reduction using accelerated acquisitions. Reconstructed images obtained from (a) single-shot EPI and (b) three-shot EPI. Panel (b) demonstrates the effect of the segmentation readout on the reduction of geometric distortions in EPI.

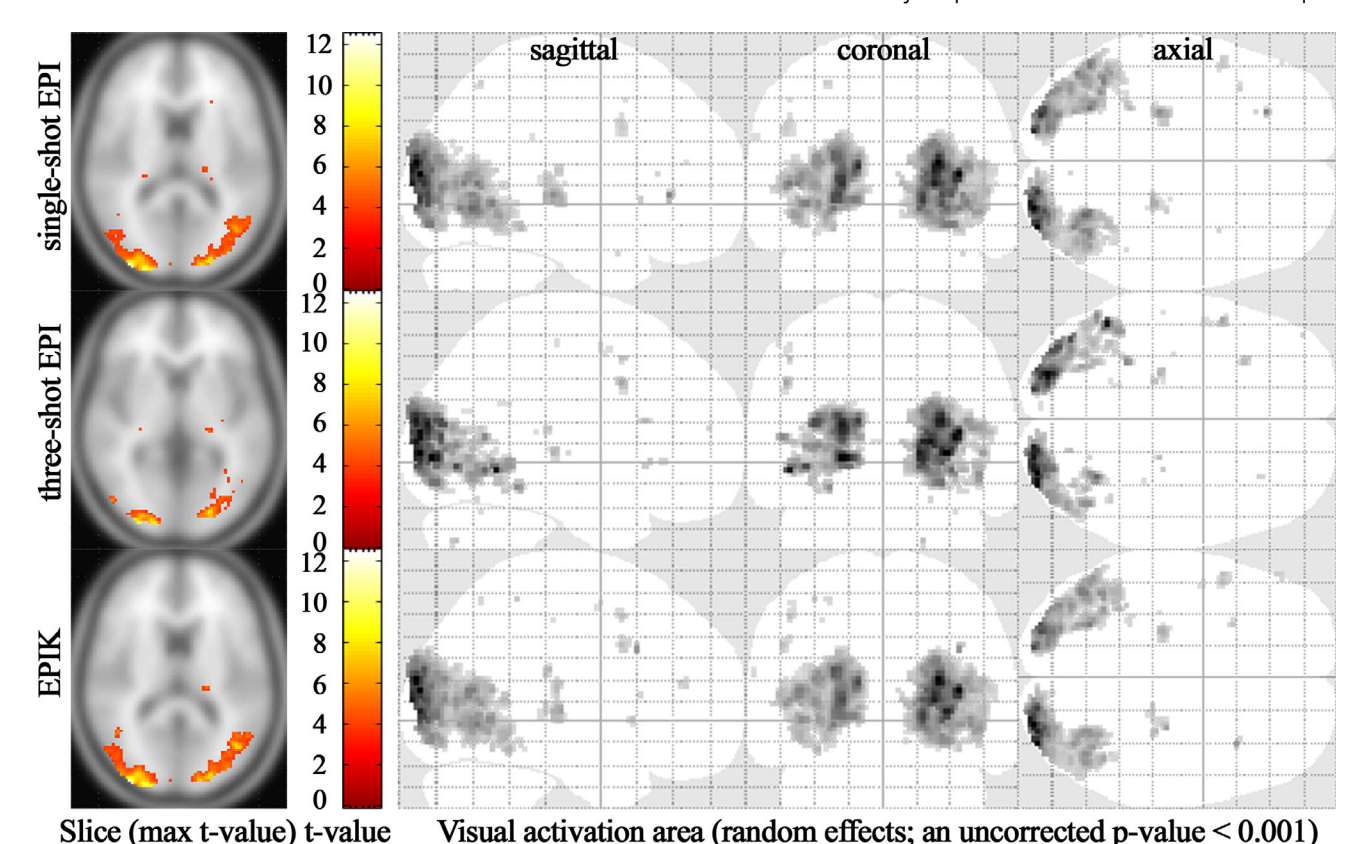


FIGURE 7: One-sample t-test results (an uncorrected *P*-value <0.001) from visual task-fMRI obtained with a group of 16 subjects. For the original fMRI time-series data acquired with 2D single-shot EPI, two other different data reconstructions (i.e. three-shot EPI and EPIK) were applied by retrospectively undersampling the *k*-space data. This figure demonstrates the effect of shot-to-shot instabilities from three-shot EPI on the fMRI activation; the activated voxels were substantially reduced in three-shot EPI (second row). However, activation results from EPIK (last row) had features very comparable to those from single-shot EPI (first row) due to the fact that EPIK fully samples the central *k*-space (keyhole region) at every scan, ensuring optimum SNR and CNR. The number of detected voxels, maximum t-value and mean t-value from the three reconstructions are 3662/2036/3672 (single-shot EPI/three-shot EPI/EPIK), 11.40/10.04/12.46 and 4.86/4.94/4.94, respectively.

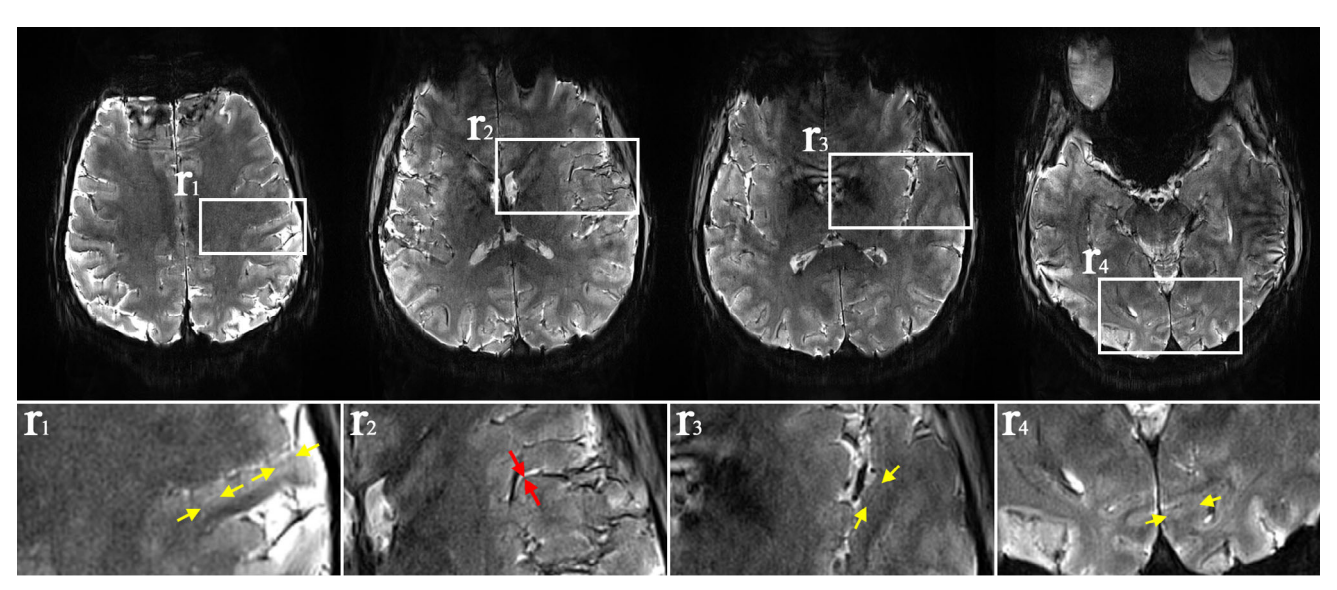


FIGURE 8: A reconstructed high-resolution functional scan obtained from a half-millimeter in-plane, 2D EPIK protocol. The protocol allowed the acquisition of functional data with a voxel size of  $0.5 \times 0.5$  mm<sup>2</sup> for 108 axial slices (1 mm thickness) under a TR of 3.5 s (see Table 2). This spatial resolution enabled the identification of the following mesoscale anatomical structures directly from a single-volume functional scan: small cerebral vessels (red arrows in  $r_2$ ) and the internal granular layer of the cortex (yellow arrows) located on the anterior wall of the postcentral gyrus ( $r_1$ ), on the Heschl gyrus ( $r_3$ ) or within the calcarine sulcus ( $r_4$ ).

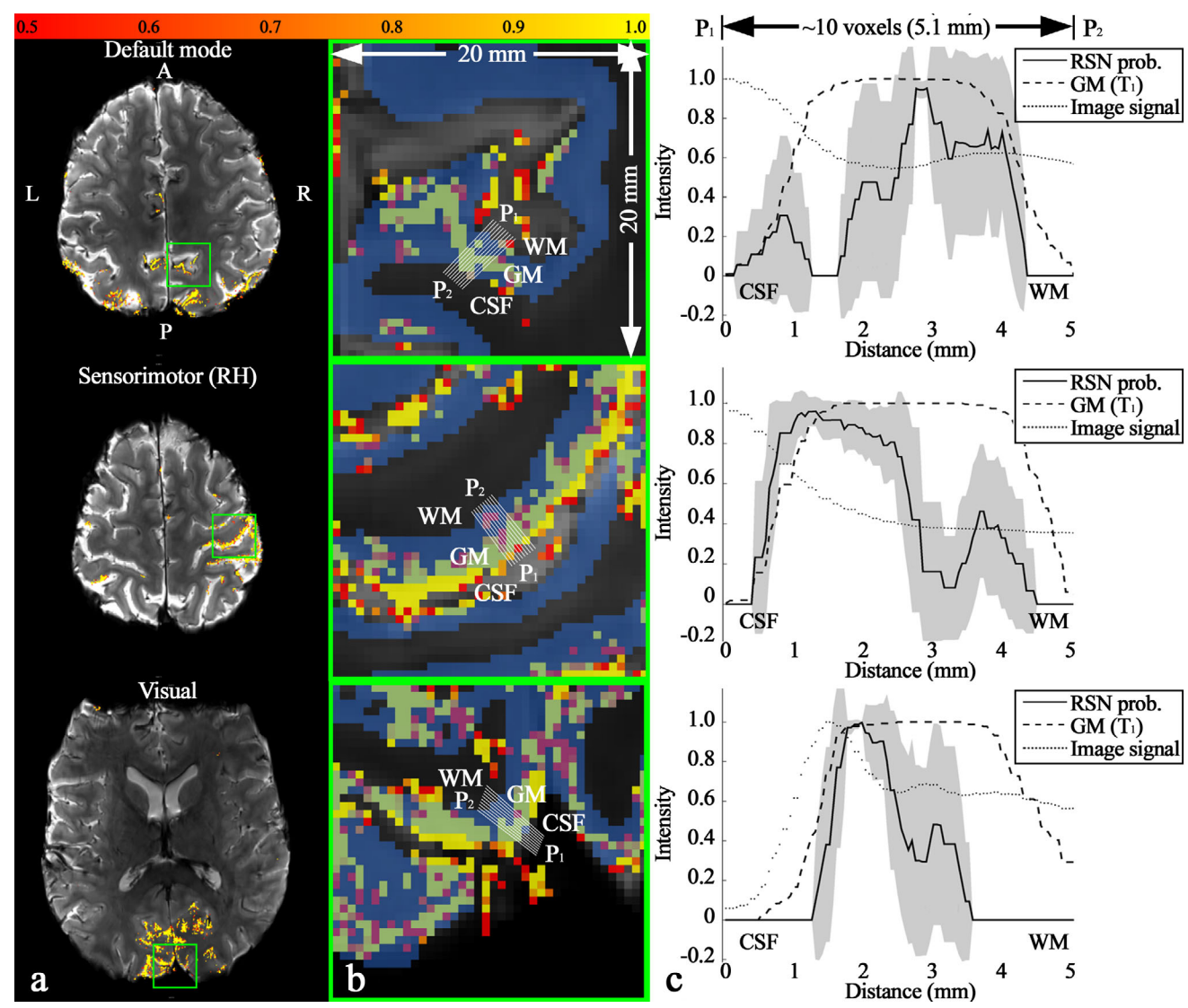


FIGURE 9: Cortical depth-dependent activation profiles obtained from a half-millimeter in-plane, 2D EPIK protocol  $(0.51 \times 0.51 \text{ mm}^2)$ . The results are depicted for the three identified resting-state networks: default mode, sensorimotor (right-hemisphere) and visual (see panel a). The mean  $\pm$  SD of the network-specific probabilities at the 20 solid lines (starting from "P<sub>1</sub>" and ending at "P<sub>2</sub>") was obtained for each network (see panel b) and is depicted in panel (c). This figure demonstrates the behavior of resting-state activation profiles with respect to the cortical depth overall, which is confined to the GM region.

comparable to that of single-shot EPI (see Fig. 7). The use of a half-millimeter in-plane protocol using EPIK for subcortical fMRI has been demonstrated; this spatial resolution enabled the identification of internal granular layer structures directly from a single fMRI scan (see Fig. 8). <sup>9,65</sup> The high spatial resolution further revealed the cortical depth-dependent functional profiles for various resting-state networks (see Fig. 9).

### 3D EVI

In 2D multi-slice EPI, data for each slice are acquired with a respective slice-selective RF excitation and subsequent 2D spatial encoding. In 3D imaging sequences, the slice-selective RF pulse is replaced with a non-selective or slab-selective RF pulse, and the excited volume is encoded with 3D spatial encoding gradients. This scheme ensures each slice is

insensitive to cross-talk artifacts between neighboring slices, which is a typical issue in 2D multi-slice imaging. Unless controlled by a technically more demanding RF pulse design, the slice profile usually achieved in a typical 2D fMRI sequence has a wider extent than expected in the slice direction. This can result in repeated partial excitation for the adjacent slice locations, and a subsequent SNR reduction is expected.<sup>34</sup> Another advantage of 3D imaging is that the phase-encoding undersampling schemes, such as parallel imaging or partial Fourier techniques, can be applied to both phase-encoding directions, which results in the high g-factor penalty, that only occurs in one phase-encoding dimension in 2D, to be spread over the two dimensions. Although accelerated multi-slice acquisition is also possible in 2D using the multi-band technique, the blipped-CAIPI method,<sup>8</sup> usually

employed for an effective unfolding of the simultaneously acquired slices, imposes an additional g-factor penalty along the same phase-encoding direction. This suggests that the combination of parallel imaging and multi-band acceleration factors needs to be chosen carefully to avoid the possible generation of significant aliasing reconstruction artifacts. <sup>66</sup>

Similar to 2D EPI, a fast imaging scheme can also be applied to 3D sequences, which samples all the data with a single-shot RF excitation and is known as 3D echo-volumar-imaging (EVI). Here, the excessively prolonged readout can dramatically increase sensitivity to field inhomogeneities, signal loss and image blurring artifacts, making the use of EVI impractical for fMRI. To overcome this, 3D GRASE uses a readout that was developed based on the Carr-Purcell-Meiboom-Gill (CMPG) SE using successive 180° pulses. This scheme can preserve signal levels better than the GE method, which is more vulnerable to the quickly decaying  $T_2^{*.53}$  When compared to 2D SE-EPI, 3D GRASE was shown to have a higher BOLD sensitivity with reduced superficial bias effect in the cortical depth functional profiles. However, stronger image blurring was evident along the partition direction (i.e. anisotropic blurring).<sup>34</sup> In 3D GRASE, the slice acquisition order can also be optimized such that the central k-space is acquired first to maximize the SNR.<sup>34</sup>

Nevertheless, for high-resolution fMRI using 3D GRASE, the readout length needs to be further shortened. In response to this, inner-volume GRASE has been suggested as it can achieve much quicker sampling by restricting the field-of-view (FOV) to only the target brain region. This is implemented by applying the refocusing gradient perpendicular to the slab excitation plane (see Fig. 4e). This restricted FOV approach allows a high spatial resolution without being affected by aliasing artifacts very much. However, the anisotropic blurring or the limited FOV in GRASE hampers its use for more general fMRI studies investigating unknown functional regions or whole-brain resting state fMRI. Several previous studies have attempted to mitigate this issue to some degree by using accelerated GRASE or its variable flip angle configuration. 40,68

# 3D EPI

An approach to overcome the long readout and associated artifacts in single-shot 3D EVI is to apply an individual RF excitation for each plane while still performing a single-shot scheme, like 2D EPI, for the spatial encoding of each plane; hence the approach is called 3D echo-"planar"-imaging (see Fig. 4f). 3D EPI has the same 3D imaging advantages over 2D, as described in the previous section, i.e. an improved slice profile or a reduced g-factor penalty with the two phase-encoding directions, but the application of parallel imaging techniques to 3D EPI can further benefit from the

CAIPIRINHA-like acceleration scheme, which yields an increased SNR at a high acceleration factor. <sup>69</sup>

However, the repeated use of an RF pulse for every plane leads to a much shorter time interval between the successive excitations on the target tissue volume, which subsequently needs a relatively low flip angle ( $\sim\!20^\circ$ ) to ensure an optimal signal level. The limited SNR from the small magnetization and be improved by acquiring a greater number of partitions, as the signal of each slice in 3D EPI is constituted by the k-space signals at all slice locations in Fourier encoding. Therefore, an intrinsic SNR advantage with a factor of  $\sqrt{N_{slice}}$  can be attained in 3D EPI at the cost of increased volumetric TR (i.e. =  $TR_{slice} \cdot N_{slice}$ ); it is important to note that a similar approach can also be applied to the 2D case by means of oversampling along the phase-encoding direction.

Due to the aforementioned benefits, 3D EPI has not only been used for BOLD fMRI, but has also been widely employed for non-BOLD fMRI studies. The effect of different 3D readout techniques (i.e. 3D GRASE and 3D EPI) on the functional sensitivity and specificity has been investigated by one previous work using both BOLD- and CBV-fMRI.<sup>2</sup> Here, 3D GRASE was shown to be effective in improving functional specificity for both contrasts, BOLD- and CBV-fMRI. However, as the CBV contrast is intrinsically more specific to the actual neural activities than BOLD, the improvement in functional specificity by means of 3D GRASE in CBV-fMRI is not as significant as the BOLD case. This may be one of the reasons why non-BOLD fMRI is performed with fewer demands on the choice of GE or SE type sequences.

One major disadvantage of 3D EPI is that its imaging scheme is also based on multiple shots, making it vulnerable to any physiological artifacts generated from subject motion, respiration or cardiac movements. The issue of physiological noise becomes more critical at UHFs due to its increasing dependence on the  $B_0$  field strength. To reduce these artifacts, several approaches have been presented, including the use of an optimal protocol configured with a reduced number of segments, or, more directly, a correction method that simultaneously measures physiological information from the subject and regresses it out from the fMRI time-series data. However, for fMRI with a very high spatial resolution, the thermal noise effect becomes more dominant, and the deleterious effects of physiological noise on shot-to-shot stabilities in 3D EPI are circumvented to some extent.

### Multi-Echo

For a single-echo fMRI technique, a TE that closely matches the  $T_2*/T_2$  of tissue is selected to deliver optimal functional contrasts. However, due to the diverse  $T_2*/T_2$  of brain tissues or the regions more sensitive to magnetic susceptibility artifacts, a single TE may not yield optimal functional detection at a certain location.<sup>74</sup> This problem can be overcome by

acquiring multiple echoes with a wider range of TEs, which can deliver increased detection extent and improved functional contrast in fMRI.<sup>75</sup> The multi-echo information can also be exploited to improve the spatial specificity by identifying venous vasculature or by extracting BOLD signals from non-BOLD components.<sup>31,76</sup>

For the effective analysis of multi-echo data, the images obtained at different TEs are combined into a single composite image using a weighted summation. The weight can be identical at all different TEs (i.e. a simple average). A recent submillimeter fMRI publication has applied the simple average to double SE-EPI and has demonstrated improved functional sensitivity in the detection of cortical depth-dependent SE-BOLD functional profiles. Other weighting methods based on the signal contrast models require quantitative mapping of  $T_2^{*75}$  or, more simply, rely on the acquired data itself (i.e. signal intensity or SNR) at given TEs. The single composition of the signal intensity or SNR) at given TEs.

While the use of multi-echo fMRI and its benefits have been successfully demonstrated with EPI-based techniques,  $^{35,74}$  the  $T_2^\prime$  contamination arising from these methods can still yield undesirable superficial bias. In response to this, another utility of multi-echo data was developed with an EPI-based readout. In this method, laminar functional profiles are less polluted by  $T_2^\prime$  by means of the recovery of fully sampled k-t space data and the reconstruction of multi-contrast images at all time points (i.e. EPTI). In another study employing a  $T_2$ -prepared conventional spoiled GE sequence, multi-echo information was exploited to extrapolate functional data back to a TE of 0 msec, resulting in distortion-absent,  $T_2$ -weighted laminar profiles free from  $T_2^\prime$  contamination.

Furthermore, a combined acquisition of GE and SE data may profit from each respective advantage (i.e. high sensitivity and specificity). However, one main disadvantage of the multi-echo technique is the long TR, which is required to accommodate all echoes within one TR interval. An optimal number of echoes or an acceleration technique may facilitate an increase in the temporal resolution and volume coverage<sup>76</sup> of the multi-echo sequences.

# Non-EPI Readout: Conventional Line-By-Line Excitation

In most fMRI techniques, the data readout is implemented based on EPI due to its very high efficiency in dynamic sampling. However, as a result of its sampling strategy, EPI images are usually degraded with several artifacts such as N/2 ghosts, geometric deformation of anatomical structures or image blurring stemming from the substantial signal decay during readout. Although some of these issues can be alleviated by means of additional post-processing or an accelerated acquisition, the artifacts develop to a more severe degree at higher field strengths, and the required correction process becomes more challenging. Therefore, an imaging method devoid of the typical EPI artifacts is favorable for more

accurate functional mapping. In view of this, one suggested approach is to use conventional line-by-line excitation imaging with a highly accelerated acquisition scheme. <sup>54,78</sup> These techniques can achieve minimal geometric distortion across the whole brain, which also assists in achieving errorless co-registration between the functional and the anatomical scans. <sup>54,55</sup>

Under this regime, the most commonly used scheme is spoiled GE (i.e. incoherent GE) due to its rather simple signal analysis model. As an alternative to this, an imaging scheme based on the coherent steady-state has been presented where the transverse magnetization between successive RF pulses is not supposed to be zero. Here, the most successful implementation of this scheme is bSSFP.55 This method has the highest SNR efficiency of all known imaging sequences and provides an SE-like BOLD contrast which is, therefore, specific to small vessels.<sup>55</sup> In addition, the fact that bSSFP does not use 180° pulses results in a reduced SAR level when compared to other SE-based methods.<sup>55</sup> However, one major issue with the bSSFP method is that its steady-state magnetization level quickly drops to nearly zero around a certain periodic range of phase offsets (i.e. stop-band), and the voxels lying within this offset range are presented as dark bands. To avoid these banding artifacts, bSSFP imaging needs to be performed with a very short TR or under a very good shim condition, which is a challenging issue at higher magnetic fields.<sup>55</sup>

Another approach to achieve the  $T_2$  contrast is to use the  $T_2$  preparation module in the GE readout method. This scheme stores the spins refocused by an 180° pulse (i.e. static field inhomogeneity eliminated) in the xz-plane and then performs the GE readout to sample the refocused signals.<sup>54</sup> As this  $T_2$  preparation module is applied once before the readout, it can avoid the high energy deposition created by a large number of refocusing pulses in a typical SE sequence.<sup>54</sup> One main drawback of the line-by-line excitation imaging is its considerably prolonged volumetric TR, which may limit its use in subcortical fMRI to partial brain coverage. 21,43 Another issue to be considered in this technique is the relatively short time interval between successive excitations. This results in a greater signal dependence on  $T_1$  relaxation time, by which, for instance, the steady-state signal of bSSFP is given as being proportional to  $\sqrt{(T_2/T_1)}$ .

### Non-Cartesian and Compressed Sensing (CS)

Sampling on the Cartesian grid provides the most straightforward image reconstruction using Fourier transform. However, it requires inefficient, regularly spaced sampling throughout the *k*-space. To achieve an even higher spatial resolution, non-Cartesian sampling strategies, such as radial or spiral trajectories, have been presented that can sample the *k*-space of a natural image more efficiently based on the fact that most energy is distributed around the central *k*-space. <sup>45,80</sup> The radial or spiral trajectories also offer increased tolerance to

Yun et al.: Layer-Specific Submillimeter fMRI Techniques

subject motion due to oversampling of the central k-space that smears out the artifacts.<sup>81</sup> However, the non-Cartesian method requires a suitable reconstruction method, which normally entails more demanding computation than the standard Fourier transform. The complex image reconstruction can also distort the time-series data, which potentially leads to the reduction of BOLD sensitivity.<sup>82</sup> Moreover, the non-Cartesian k-space traversal is more susceptible to offresonance artifacts, ultimately leading to blurring and reduced robustness. Thus, specific correction<sup>80</sup> or self-navigating methods<sup>45</sup> are required to ensure the accurate localization of the functional activity, and, as a result, the use of non-Cartesian methods has been demonstrated for subcortical fMRI. 45 The performance of non-Cartesian imaging also relies on the performance of the hardware. The related issues, such as gradient delays or eddy currents, can hamper image quality, and therefore, an extra calibration scan may be necessary to assess the degree of the artifacts. Here, an autocalibrated approach has shown its utility in correcting the artifacts without the need for the extra calibration scan.<sup>83</sup>

A larger acceleration factor is also possible using the random sampling approach, generally referred to as CS,<sup>84</sup> which can achieve a significant improvement in the spatial resolution. However, its use for fMRI may raise additional concerns, such as potential loss of functional detection efficiency or an increased temporal correlation of time-series data from the nonlinear reconstruction process.<sup>85</sup>

# Restricted FOV Imaging

The restriction of the FOV allows the more straightforward implementation of a high-resolution protocol as it does not need to reconstruct a full-FOV image, which can potentially generate additional reconstruction artifacts. This technique can be categorized into two classes: inner-volume selection (IVS) and outer-volume suppression (OVS).

A representative IVS technique is 3D GRASE using the spatially orthogonal slab selective gradient pairs for the excitation and refocusing pulses. Another IVS technique is the use of a spatially selective RF pulse that can only excite a selected local region-of-interest (ROI). Using this technique, previous works have demonstrated a very high spatial resolution for fMRI, such as  $0.5 \times 0.5 \text{ mm}^{2.86}$  Although the spatial resolution is sufficiently high to reveal cortical depth-dependent activation, to the best of our knowledge, its use has not yet been demonstrated for the delineation of subcortical activation patterns. The rare use of this technique is mainly attributed to the technical difficulties associated with the RF pulse design; a relatively long RF pulse duration is often required for a sharp excitation profile, and the subsequently increased off-resonance effects induce a loss of spatial resolution.<sup>87</sup> The long RF pulse duration can be shortened using an RF acceleration technique (eg transmit-SENSE),88 which, however,

requires additional hardware equipment, i.e. a parallel transmission system.

The OVS technique restricts the FOV by suppressing the signals outside the ROI with spatially selective pulses followed by dephasing gradients. Based on this scheme, previous work proposed Zoomed-GRAPPA imaging, which has achieved a 0.65 mm isovoxel for high-resolution fMRI. Another technique utilizing the OVS scheme is the line-scanning method, which only acquires data for a very limited ROI without a phase-encoding. This method offers the unique advantage of measuring mesoscale functional response with a few hundred milliseconds of temporal resolution. Previous work has demonstrated its use for investigating time-resolved cognitive computations with laminar precision.

# Supplementary Techniques for Accurate Spatial Mapping

### Correction of Geometric Distortion in EPI

For EPI-based fMRI techniques, accurate mapping of activated voxels is often hindered by the geometric deformation of tissue structures typically seen in the reconstructed images. Geometric distortion is more apparent in the phase-encoding direction due to the much slower acquisition (i.e. lower bandwidth) than in the frequency-encoding.

Distortion can be corrected using a direct measurement of the  $B_0$  offset or the PSF of the employed EPI protocol. <sup>91</sup> However, this approach requires other types of imaging sequences, which may not be available in a commercial scanner. Instead, another widely used method is to acquire EPI data with an opposite phase-encoding direction, which registers the image voxels between the two different encoding-direction data and subsequently relocates the shifted voxels onto the correct grid. 92 The inversion of the phase-encoding direction can be easily accomplished by rotating the FOV in the sequence interface, and the required phase-inverted data are a few temporal volumes  $(3 \sim 5 \text{ scans})$ , meaning that only a minimal time increase for the extra scan is required. Several software packages, such as COPE (Brain Voyager) (https://support.brainvoyager.com/ brainvoyager/available-tools/86-available-plugins/62-epi-distortio n-correction-cope-plugin), ANTs (https://github.com/ANTsX/ ANTs), 3DQwarp (AFNI) (https://afni.nimh.nih.gov/pub/dist/ doc/program\_help/3dQwarp.html), and TOPUP (FSL) (https:// fsl.fmrib.ox.ac.uk/fsl/fslwiki/topup) are available for this correction scheme, and its use has been demonstrated in numerous subcortical BOLD and non-BOLD fMRI studies. 13,19,33,36

Figure 10 shows an exemplary result of the distortion correction, in which more accurate co-registration and functional mapping onto the anatomical scan can be observed. Although this example does not depict any significant visible loss of spatial resolution, previous works have reported that the distortion correction errors generated from this unwarping process (i.e. resampling or interpolation of the voxels) may

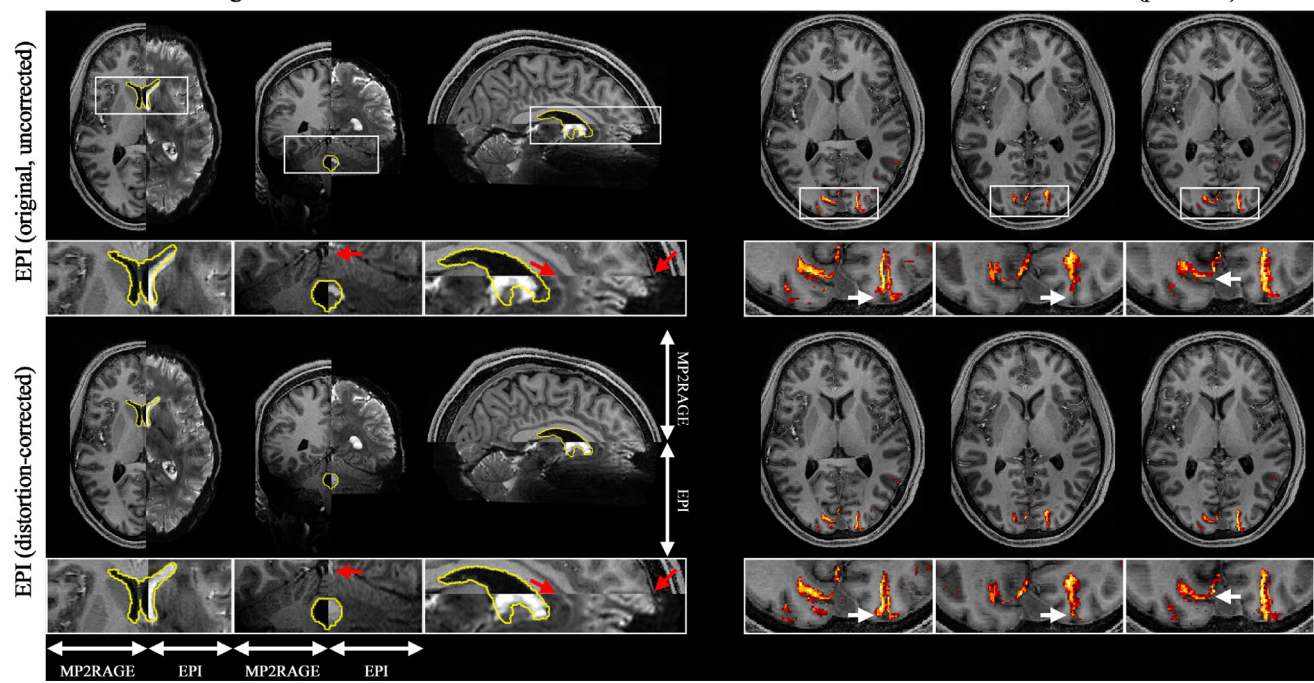


FIGURE 10: The effect of EPI geometric distortion corrections on the co-registration and functional mapping. (a) Depicts improved co-registration between MPRAGE and EPI in the distortion-corrected case around the regions marked by yellow circles (i.e. ventricles) and red arrows (see the enlarged depiction of the selected ROIs shown below in each slice). As a result, the activated voxels are also more accurately localized along the cortical ribbon (see the white arrows in [b]) when compared to the non-corrected case.

yield reduced spatial specificity or introduce additional spatial correlation into the time-series, which then deteriorates the cortical depth-dependent functional signals. 41,94

### Distortion-Matched Anatomical Scan

For the reasons described above, sometimes a more attractive solution than distortion correction is to acquire a distortionmatched anatomical scan using the same base sequence as for the fMRI acquisition (i.e. EPI). The definition of the cortical boundaries from the anatomical scan is particularly important for subcortical functional analysis to enable the location of cortical layers or columns to be determined. However, a typical EPI protocol used in fMRI does not have sufficient structural contrast to segment the cortical regions out of other tissue components. 42 Therefore, to acquire an anatomical scan using EPI, a contrast preparation module, such as inversion or magnetization transfer, is used, which can deliver the magnetization-prepared, rapid GE (MPRAGE)-like  $T_1$  contrast. <sup>42,95</sup> In this way, the  $T_1$ weighted, anatomical EPI scan has distortions identical to the fMRI data, resulting in errorless co-registration between the anatomical and functional scans.<sup>95</sup>

The feasibility of using this technique for subcortical fMRI has been demonstrated previously.<sup>32,41</sup> Importantly, however, it should be noted that the anatomical reference also has the same EPI geometric distortions. This indicates that the method may not be suitable for other analyses relying on anatomical information, such as the morphometric

measurement of cortical thickness or the cortical surface-based atlasing.  $^{94}$  Here, the distortion of  $T_1$ -weighted EPI can also be reduced by using the same distortion correction approach as described in the previous section, although it requires an additional increase in acquisition time.

# Reduction of Large Vessel Effect in GE-BOLD

When compared to SE-BOLD or non-BOLD fMRI, the GE-BOLD fMRI technique has an increased detection sensitivity for neural activities along with a reduced RF energy deposition, which is beneficial at high magnetic fields. <sup>13,33</sup> For this reason, while maintaining the advantages of GE-BOLD, previous works have suggested correcting the superficial bias effect for more accurate characterization of subcortical activation profiles.

One approach is to directly identify the anatomical locations of the veins and to remove the venous voxels from the functional analysis. Here, for the effective identification of venous structures, an extra anatomical scan using susceptibility-weighted imaging (SWI) can be used. Another method is the use of the vascular model for the BOLD signal. As illustrated in Fig. 5, the BOLD signals at a certain layer can be formulated as the functional signals at the local activation site plus the weighted summation of those from the deeper layers (i.e. non-local activation) delivered by the ascending veins. Based on this model, previous work has derived the weighting factors and has performed spatial deconvolution to remove the

draining vein effects. 11,13 However, the above correction methods require prior knowledge of the vein location or the vascular model, which may require an additional scan.

In contrast, a data-driven method has also been presented that only relies on measured functional data. Here, the underlying principle is that the magnitude BOLD signals are contributed by both small and large vessels, while the phase data are primarily only affected by large vessels. Therefore, the method regresses out the phase component from the functional data by first fitting the phase to the magnitude data and then subtracting the resultant maximum likelihood estimator to remove the signal components attributed to the large veins. Previous work has verified its use for subcortical fMRI, in which the phase-regressed GE-BOLD activation pattern was shown to be similar to that of SE-EPI.

An alternative fMRI analysis method to eliminate the effect of other vascular sources, i.e. different baseline physiological parameters (eg CBV or  $T_2$ \*) depending on cortical depth has also been presented (see Fig. 5). As these parameters are assumed to act as a multiplicative factor to the BOLD signals, the method proposes the normalization of the effect by taking the division of the two stimulus conditions in the fMRI analysis, rather than the subtraction typically used in most functional analyses. (41)

### Discussion

# Summary of Subcortical fMRI Techniques

For the delineation of subcortical functional activation, numerous fMRI techniques have been developed based on the exploitation of a specific functional contrast (see Section 'fMRI Contrasts') in combination with a dedicated imaging technique (see Section 'Sub-mm fMRI Techniques'). Due to its relatively high functional detection sensitivity and low SAR level, one widely used combination is BOLD contrast acquired with GE-EPI. Here, the superficial bias effect arising from the large draining veins can be resolved by replacing the GE readout with the SE readout, the use of which, however, may be restrictive for whole-brain fMRI due to the increased SAR caused by the refocusing pulse. Instead, the spatial specificity of GE-BOLD can be improved by applying a superficial bias correction method, which has been shown to provide SE-like activation patterns.<sup>31</sup>

The imaging techniques using non-BOLD contrasts are also sensitized to detect functional signals proximal to neuronal activation. However, similar to the SE-BOLD technique, the inversion recovery or tagging pulses, designed to create functional contrasts in the non-BOLD techniques, result in a substantial increase in volumetric TR and SAR. <sup>13,33</sup> Previous works have benchmarked the performance of three different fMRI methods (GE-BOLD, SE-BOLD, VASO) and have reported that VASO showed poor levels of accuracy in decoding the orientation of feedforward and feedback signals

in visual fMRI, <sup>12</sup> which may be attributed to the lower statistical power brought about by the lower temporal resolution. While VASO was shown to be spatially more specific to the subcortical functional activation, this advantage comes with the trade-off of reduced functional sensitivity (i.e.  $2 \sim 8$  times lower z-values for the same amount of data). <sup>13,29</sup>

At UHFs, the increased SNR and functional CNR facilitates high-resolution fMRI with enhanced spatial specificity and, to date, most subcortical fMRI studies have been performed under this circumstance. Nevertheless, intrinsic properties or technical challenges arising from the use of UHF may be a limiting factor, depending on the specific fMRI techniques used. For EPI-based techniques, the fact that the increased  $B_0$  inhomogeneities and a shorter  $T_2$ \* create geometric distortions, signal loss or blurring artifacts demands careful consideration of imaging protocol or higher-order shimming. The geometric distortions are often further corrected with an additional correction method that uses the reversed phase-encoding data. On the other hand, the  $B_1$ inhomogeneity at UHF becomes a critical issue for techniques using high flip angles (eg 2D SE-EPI, 3D GRASE or non-BOLD imaging) and may possibly result in a decrease in the BOLD functional connectivity. 97 To account for this issue, the use of an additional calibration scan (i.e.  $B_1$  mapping) and RF optimization with a parallel transmission system have been attempted. 34,88 The increased field strength also causes an increase in the  $T_1$  relaxation time, which may result in a longer contrast-preparation time in the non-BOLD techniques that rely on the inversion recovery of targeted spins.

To achieve high spatial resolution in fMRI, more efficient k-space sampling using non-Cartesian trajectories or CS can be used. However, the complex image reconstruction (eg reduced statistical degree of freedom from a regularized reconstruction) or off-resonance artifacts may distort the functional signals, thus impairing its use for subcortical fMRI unless an effective correction method is applied.  $^{9,45,80,82,85}$  Alternatively, a more robust, distortion-free k-space sampling method (eg bSSFP or FLASH) using the conventional GE sequences has also been proposed. This line-by-line excitation scheme can attain much purer  $T_2$  functional contrast without being plagued by the geometric distortions typically observed in EPI. However, the excessively long acquisition time suggests its use only in circumstances where reduced temporal resolution or limited brain coverage can be tolerated.

In a conventional 2D line-by-line excitation sequence, the relatively short TR (i.e. a few tens of milliseconds) may raise concerns relating to the inflow effect. This is an additional signal change created by unsaturated blood flowing into the slice, known as the time-of-flight (TOF) effect. However, the effect is only significant at a relatively short TR, during which the traveled distance of the spins is shorter than the slice thickness. Therefore, in the case of 2D multislice EPI, most fMRI protocols that use a relatively long TR

(i.e. >1 s) can be employed with little concern for the inflow effect, as demonstrated by previous works. 98

In contrast, 3D EPI is inherently free from the inflow effect as the whole brain volume is always excited between successive RF excitations. Other advantages of 3D imaging over 2D imaging are the perfect slice profile obtained and the possibility of applying in-plane acceleration techniques along two phase-encoding directions. When compared to single-shot-based 3D EVI, 3D EPI has a higher SNR and increased brain coverage and hence, is widely used for fMRI. However, the multi-shot scheme of 3D EPI has increased susceptibility to physiological noise and motion artifacts, potentially causing reduced temporal SNR or poor seed-based correlation performance in resting-state fMRI (rs-fMRI) unless controlled with an additional correction method. 71,72

As summarized above, each fMRI technique has advantages and disadvantages according to various assessment criteria, and currently, there is no particular subcortical fMRI technique that is overwhelmingly outstanding compared to other techniques. Therefore, depending on the purpose of the study, the most appropriate functional contrast and readout technique needs to be carefully determined. For example, when a robust high-resolution method with whole-brain coverage is important, GE-BOLD with an EPIK readout incorporating bias correction would be a good choice. Conversely, when spatial specificity is paramount, the non-BOLD contrasts or SE-BOLD using 2D SE-EPI or 3D GRASE techniques would be good candidates. For non-BOLD fMRI, SE readout is not essential to improve spatial specificity, and 3D EPI has been favorably employed in most cases. However, other readout methods can possibly be applied to mandate the corresponding imaging benefits. In this review, we have mainly focused on the introduction of submillimeter fMRI acquisition techniques. Data sets acquired with this level of high spatial resolution usually require a dedicated pre-processing or data analysis approach for more accurate functional mapping. 94,99 This is, however, beyond the scope of the current work and is hence not discussed herein.

# Functional Resolution and Spatial Resolution of the Sequence

The complex nature of the neuronal hemodynamic response is manifest in that neural activation, closely linked to an increase in CMRO<sub>2</sub>, also induces changes in the blood supply. Here, the architecture of the vascular network plays an important part in the interpretation of fMRI signals. For instance, the heterogeneous distribution of cerebral veins and venules induces a spatial blurring of functional signals, which is more pronounced in the GE-BOLD studies. Another factor that affects the functional resolution is the varying capillary density. Previous studies have shown that enhanced spatial specificity can be achieved at higher fields and shorter TEs because the relative contribution of the microvasculature to

the functional signals over that of macrovasculature increases under these circumstances.<sup>6</sup> Attempts to evaluate the functional resolution were made by estimating the hemodynamic PSF. In a photo-stimulation study using mice, the full-widthat-half-maximum (FWHM) of the hemodynamic PSF was shown to be in the range of between 0.103 mm and 0.175 mm. 100 In another study relating to a human ocular dominance column, the FWHM of the PSF for GE-BOLD and SE-BOLD was assessed as 0.99 mm and 0.86 mm, respectively. 101 Despite contentious discussions around the functional resolution, the detection of subcortical functional activation has been demonstrated in numerous submillimeter fMRI studies. A recently published study has also successfully revealed the cortical depth-dependent profiles for whole-brain, restingstate networks, in which the functional data were processed using standard pre-processing steps and the GE-bias correction method, and no further contamination was introduced through additional data polishing techniques.<sup>9</sup>

In high-resolution EPI using a relatively large imaging matrix size, the consequent long acquisition window is often shortened with the partial Fourier technique to reduce the  $T_2$ \* decay effect. However, if the missing k-space from partial Fourier imaging is poorly estimated, the technique can introduce additional spatial blurring. 9,102 This effect can be minimized when a large imaging matrix size and a more sophisticated reconstruction method are employed, as demonstrated previously (see Fig. 11). In addition, for the same accelerated EPI protocol, the reconstructed image quality or SNR can be improved by means of different image reconstruction software. Previous work has demonstrated that the aliasing artifacts observed in the original EPI images were significantly eliminated using other inhouse developed image reconstruction routine.<sup>66</sup> Therefore, in practice, the choice of imaging protocol and a reconstruction method can have a critical impact on the spatial resolution or the reconstructed image quality.

# Quality Control in Subcortical fMRI

For the reliable and reproducible detection of subcortical functional signals, the quality of submillimeter fMRI data needs to be carefully controlled. In general, the quality control (QC) procedure for fMRI requires various assessment tasks to be performed, depending on the purpose of the study and the stage of the experiment. <sup>103</sup> This sub-section describes QC criteria that directly relate to the assessment of submillimeter fMRI data.

During the study planning stage, it is important to employ a robust imaging protocol to yield a reconstructed image of sufficient quality as submillimeter fMRI data usually suffer from relatively low image SNR and associated image artifacts. Therefore, a protocol using a relatively high acceleration factor (eg eight-fold GRAPPA<sup>104</sup>) may not be suitable in a study where a robust image quality is required. Moreover, when an EPI-based technique is used, PSF analysis may also be necessary to evaluate the degree of spatial resolution

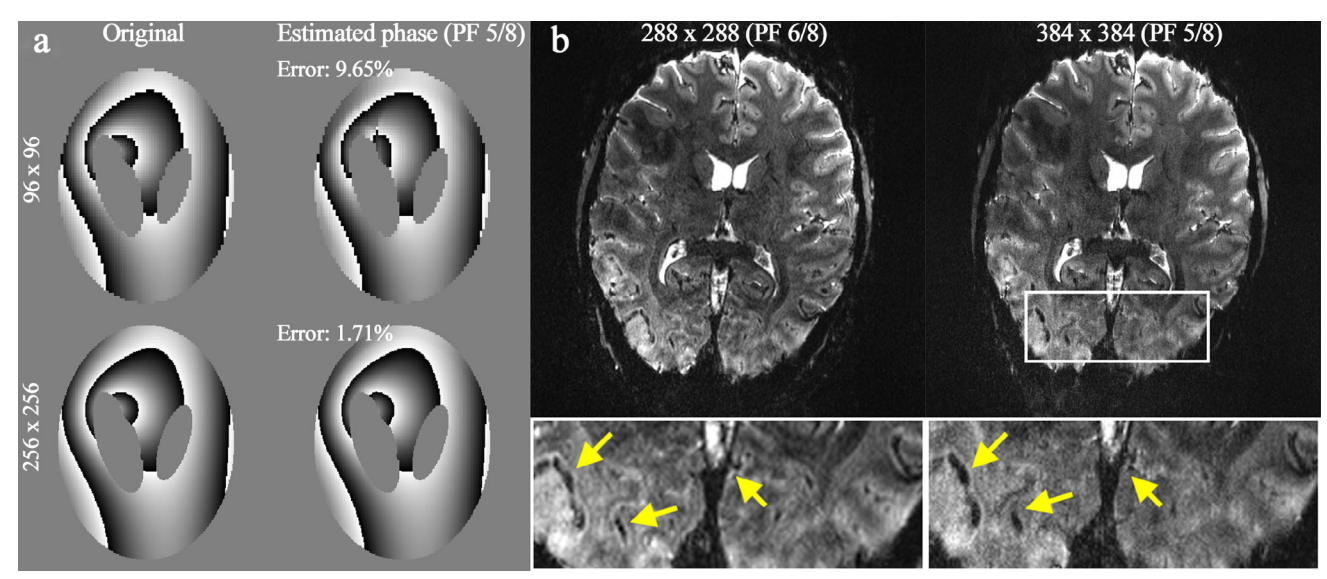


FIGURE 11: The effect of a large imaging matrix size on partial Fourier reconstruction. (a) Simulation results of the phase estimation for partial Fourier undersampled data with a factor of 5/8 (top:  $96 \times 96$  and bottom:  $256 \times 256$ ). For the larger matrix size case, the estimated phase profile (right column) is nearly identical to that of the original phase (left column), whereas the smaller matrix size case depicts substantial differences from each other. (b) Partial-Fourier-accelerated 2D GE-EPI obtained with the following conditions:  $384 \times 384$  with a factor of 5/8 (left column) and  $288 \times 288$  with a factor of 6/8 (right column). Albeit at the larger partial Fourier factor, the spatial resolution of the left image is observed to be better than that of the right image due to the use of a larger matrix size; see the yellow arrows in the enlarged depiction of the selected ROI.

blurring<sup>9,19</sup> created by the  $T_2/T_2$ \* decay during the relatively long acquisition window. For an improved subcortical data analysis, physiological noise information is often simultaneously recorded during the fMRI acquisition. In this regard, prior to scanning, care must be taken to ensure a secure contact between the recording devices and subjects.

During the data processing stage, an initial evaluation of the acquired data is required to check the quality of reconstructed images. Here, the image SNR and tSNR offer a metric to assess the signal level and temporal stabilities through the time series. The carpet plot 105 is also useful for the visual detection of abrupt signal changes caused by motion or any other sources. More quantitatively, the displacement calculated from typical realignment processing can be used as a numerical criterion (eg mean displacement < 0.5 mm) so that only data sets having acceptable motion ranges for reliable detection of submillimeter functional signals for a group of subjects are included in the data set. 9 The temporal skewness<sup>37</sup> can also provide an effective indication with which to detect intermittent ghosting artifacts. Furthermore, during the fMRI analysis, a high mapping fidelity can be assured by computing the spatial correlation between the acquired activated voxels and the reference atlas template.

# Future Direction: Spatiotemporal Resolution and Brain Coverage of Subcortical fMRI

Advancements in fMRI techniques over the last decade have ultimately been aimed toward the detection of functional signals with a time-resolved and a layer-specific spatial scale to reveal the organization of neural circuits in the brain. The

development of current fMRI techniques allows the acquisition of functional signals with a submillimeter voxel size, but usually with a relatively slow temporal resolution (3  $\sim$  5 s). Furthermore, most subcortical fMRI studies have only targeted particular brain regions evoked by a specific task paradigm, which precludes the possibility of the analysis of whole-brain connectivity.

In contrast to task-evoked fMRI, rs-fMRI identifies overall activity in the brain and the associated underlying connectivity. The task-free acquisition also ensures its straightforward use for all types of subjects, including patients or children, where brain function and the characteristics thereof are of great interest in clinical applications. To facilitate the various analysis approaches suggested for rs-fMRI (eg regional homogeneity, functional connectivity density or independent component analysis), whole-brain coverage is demanded as the first requirement in rs-fMRI. In early work, several submillimeter protocols were proposed to investigate subcortical functional profiles for rs-fMRI: Guidi<sub>2020</sub> (1.15 mm<sup>3</sup>; 10 slices; 1.65 s),<sup>48</sup> Huber<sub>2021</sub>  $(0.51 \text{ mm}^3; 72 \sim 104 \text{ slices}; 6.5 \sim 8 \text{ s}),^{47} \text{ Deshpande}_{2022}$  $(1.08 \text{ mm}^3; 37 \text{ slices}; 3 \text{ s}),^{30} \text{ and } \text{Yun}_{2022} (0.25 \text{ mm}^3;$ 123 slices; 3.5 s),9 where the parameters presented in the parenthesis show the achieved single-voxel volume, slices and temporal resolution provided in each study.

The above subcortical rs-fMRI employed a relatively long TR. However, the fact that rs-fMRI focuses on low-frequency fluctuations (<0.1 Hz; Nyquist sampling upper limit of 5 s) still makes conventional data analyses feasible. <sup>9,37</sup> Although reducing the temporal sampling efficiency, a long TR measurement can increase the spatial resolution or brain

coverage with an improved SNR. Conversely, a shorter TR allows the acquisition of functional data with a greater number of dynamic samples, resulting in an increased degree of freedom and a potential improvement in the regressor fitting. <sup>106</sup> However, the shorter time constraint for each slice encoding leads to reduced spatial resolution or reduced brain coverage along with a lower SNR level when compared to a longer TR case with otherwise identical imaging conditions. Notwithstanding the current advance of fMRI techniques, the community need for a deeper understanding of brain functions fosters the growth of further improvements in imaging techniques toward higher spatiotemporal resolution, which supports any type of functional study.

# Acknowledgments

The authors would like to thank the efforts of Claire Rick for English proofreading. This research did not receive any specific grant from funding agencies in the public, commercial, or not-for-profit sectors. Open Access funding enabled and organized by Projekt DEAL.

# **Conflict of Interest**

The authors declare no competing interests.

### References

- Ogawa S, Lee TM, Kay AR, Tank DW. Brain magnetic resonance imaging with contrast dependent on blood oxygenation. Proc Natl Acad Sci U S A 1990;87(24):9868-9872.
- Beckett AJS, Dadakova T, Townsend J, Huber L, Park S, Feinberg DA. Comparison of BOLD and CBV using 3D EPI and 3D GRASE for cortical layer functional MRI at 7 T. Magn Reson Med 2020;84(6):3128-3145.
- Kim SG, Uğurbil K. Comparison of blood oxygenation and cerebral blood flow effects in fMRI: Estimation of relative oxygen consumption change. Magn Reson Med 1997;38(1):59-65.
- Lu H, Golay X, Pekar JJ, Van Zijl PC. Functional magnetic resonance imaging based on changes in vascular space occupancy. Magn Reson Med 2003;50(2):263-274.
- Davis TL, Kwong KK, Weisskoff RM, Rosen BR. Calibrated functional MRI: Mapping the dynamics of oxidative metabolism. Proc Natl Acad Sci U S A 1998;95(4):1834-1839.
- Yacoub E, Duong TQ, Van De Moortele PF, et al. Spin-echo fMRI in humans using high spatial resolutions and high magnetic fields. Magn Reson Med 2003;49(4):655-664.
- Griswold MA, Jakob PM, Heidemann RM, et al. Generalized autocalibrating partially parallel acquisitions (GRAPPA). Magn Reson Med 2002;47(6):1202-1210.
- Setsompop K, Gagoski BA, Polimeni JR, Witzel T, Wedeen VJ, Wald LL. Blipped-controlled aliasing in parallel imaging for simultaneous multislice echo planar imaging with reduced g-factor penalty. Magn Reson Med 2012;67(5):1210-1224.
- Yun SD, Pais-Roldán P, Palomero-Gallagher N, Shah NJ. Mapping of whole-cerebrum resting-state networks using ultra-high resolution acquisition protocols. Hum Brain Mapp 2022;43(11):3386-3403.
- De Martino F, Zimmermann J, Muckli L, Ugurbil K, Yacoub E, Goebel R. Cortical depth dependent functional responses in humans at 7T: Improved specificity with 3D GRASE. PloS One 2013;8(3): e60514.

- Marquardt I, Schneider M, Gulban OF, Ivanov D, Uludağ K. Cortical depth profiles of luminance contrast responses in human V1 and V2 using 7 T fMRI. Hum Brain Mapp 2018;39(7):2812-2827.
- Iamshchinina P, Haenelt D, Trampel R, Weiskopf N, Kaiser D, Cichy RM. Benchmarking GE-BOLD, SE-BOLD, and SS-SI-VASO sequences for depth-dependent separation of feedforward and feedback signals in high-field MRI. bioRxiv 2021; https://doi.org/10.1101/ 2021.12.10.472064.
- de Hollander G, van der Zwaag W, Qian C, Zhang P, Knapen T. Ultrahigh field fMRI reveals origins of feedforward and feedback activity within laminae of human ocular dominance columns. Neuroimage 2021;228:117683.
- Berlot E, Arts R, Smit J, et al. A 7 Tesla fMRI investigation of human tinnitus percept in cortical and subcortical auditory areas. Neuroimage Clin 2020;25:102166.
- Huber L, Uludağ K, Möller HE. Non-BOLD contrast for laminar fMRI in humans: CBF, CBV, and CMRO<sub>2</sub>. Neuroimage 2019;197:742-760.
- Lee SP, Silva AC, Ugurbil K, Kim SG. Diffusion-weighted spin-echo fMRI at 9.4 T: Microvascular/tissue contribution to BOLD signal changes. Magn Reson Med 1999;42(5):919-928.
- Gusnard DA, Raichle ME, Raichle ME. Searching for a baseline: Functional imaging and the resting human brain. Nat Rev Neurosci 2001; 2(10):685-694.
- Shao X, Guo F, Shou Q, et al. Laminar perfusion imaging with zoomed arterial spin labeling at 7 Tesla. bioRxiv 2021; https://doi.org/10.1101/ 2021.04.13.439689.
- Kashyap S, Ivanov D, Havlicek M, Huber L, Poser BA, Uludağ K. Submillimetre resolution laminar fMRI using arterial spin labelling in humans at 7 T. PloS One 2021;16(4):e0250504.
- Taso M, Munsch F, Zhao L, Alsop DC. Regional and depth-dependence of cortical blood-flow assessed with highresolution arterial spin labeling (ASL). J Cereb Blood Flow Metab 2021;41(8):1899-1911.
- 21. Koopmans PJ, Barth M, Norris DG. Layer-specific BOLD activation in human V1. Hum Brain Mapp 2010;31(9):1297-1304.
- 22. Guidi M, Huber L, Lampe L, Gauthier CJ, Möller HE. Lamina-dependent calibrated BOLD response in human primary motor cortex. Neuroimage 2016;141:250-261.
- Huber L, Finn ES, Handwerker DA, et al. Sub-millimeter fMRI reveals multiple topographical digit representations that form action maps in human motor cortex. Neuroimage 2020;208:116463.
- Kim T, Kim SG. Quantification of cerebral arterial blood volume and cerebral blood flow using MRI with modulation of tissue and vessel (MOTIVE) signals. Magn Reson Med 2005;54(2):333-342.
- Gauthier CJ, Hoge RD. A generalized procedure for calibrated MRI incorporating hyperoxia and hypercapnia. Hum Brain Mapp 2013; 34(5):1053-1069.
- Chiarelli PA, Bulte DP, Wise R, Gallichan D, Jezzard P. A calibration method for quantitative BOLD fMRI based on hyperoxia. Neuroimage 2007;37(3):808-820.
- Grubb RL Jr, Raichle ME, Eichling JO, Ter-Pogossian MM. The effects
  of changes in PaCO2 on cerebral blood volume, blood flow, and vascular mean transit time. Stroke 1974;5(5):630-639.
- Kay K, Jamison KW, Vizioli L, Zhang R, Margalit E, Ugurbil K. A critical assessment of data quality and venous effects in sub-millimeter fMRI. Neuroimage 2019;189:847-869.
- Haenelt D, Weiskopf N, Vaculciakova L, et al. Mapping ocular dominance columns in humans using GE-EPI, SE-EPI and SS-SI-VASO at 7 T. Proceedings of the Virtual Conference of ISMRM; 2020. (abstract 1230).
- Deshpande G, Wang Y, Robinson J. Resting state fMRI connectivity is sensitive to laminar connectional architecture in the human brain. Brain Inform 2022;9(1):2.

#### Yun et al.: Layer-Specific Submillimeter fMRI Techniques

- Stanley OW, Kuurstra AB, Klassen LM, Menon RS, Gati JS. Effects of phase regression on high-resolution functional MRI of the primary visual cortex. Neuroimage 2021;227:117631.
- Navarro KT, Sanchez MJ, Engel SA, Olman CA, Weldon KB. Depthdependent functional MRI responses to chromatic and achromatic stimuli throughout V1 and V2. Neuroimage 2021;226:117520.
- Huang P, Correia MM, Rua C, Rodgers CT, Henson RN, Carlin JD. Correcting for superficial bias in 7T gradient echo fMRI. Front Neurosci 2021;15:715549.
- Kemper VG, De Martino F, Vu AT, et al. Sub-millimeter T2 weighted fMRI at 7 T: Comparison of 3D-GRASE and 2D SE-EPI. Front Neurosci 2015;9:163.
- Han S, Eun S, Cho H, Uludağ K, Kim SG. Improved laminar specificity and sensitivity by combining SE and GE BOLD signals. Neuroimage 2022;264:119675.
- Wang F, Dong Z, Wald LL, Polimeni JR, Setsompop K. Simultaneous pure T2 and varying T2'-weighted BOLD fMRI using echo planar timeresolved imaging for mapping cortical-depth dependent responses. Neuroimage 2021;245:118641.
- Berman AJL, Grissom WA, Witzel T, et al. Ultra-high spatial resolution BOLD fMRI in humans using combined segmented-accelerated VFA-FLEET with a recursive RF pulse design. Magn Reson Med 2021;85(1): 120-139.
- Pais-Roldán P, Yun SD, Palomero-Gallagher N, Shah NJ. Cortical depth-dependent human fMRI of resting-state networks using EPIK. Front Neurosci 2023;17:1151544. https://doi.org/10.3389/fnins.2023. 1151544.
- Yun SD, Pais-Roldán P, Shah NJ. Detection of cortical depthdependent functional activation using whole-brain, half-millimetre resolution EPIK at 7T. Proceedings of the Virtual Conference of ISMRM; 2020. (abstract 3863).
- Park S, Torrisi S, Townsend JD, Beckett A, Feinberg DA. Highly accelerated submillimeter resolution 3D GRASE with controlled T2 blurring in T2-weighted functional MRI at 7 Tesla: A feasibility study. Magn Reson Med 2021;85(5):2490-2506.
- Kashyap S, Ivanov D, Havlicek M, Poser BA, Uludağ K. Impact of acquisition and analysis strategies on cortical depth-dependent fMRI. Neuroimage 2018;168:332-344.
- Chai Y, Li L, Wang Y, et al. Magnetization transfer weighted EPI facilitates cortical depth determination in native fMRI space. Neuroimage 2021;242:118455.
- Pfaffenrot V, Voelker MN, Kashyap S, Koopmans PJ. Laminar fMRI using T2-prepared multi-echo FLASH. Neuroimage 2021;236:118163.
- Morgan AT, Nothnagel N, Petro LS, Goense J, Muckli L. Highresolution line-scanning reveals distinct visual response properties across human cortical layers. bioRxiv 2020; https://doi.org/10.1101/ 2020.06.30.179762.
- Graedel NN, Miller KL, Chiew M. Ultrahigh resolution fMRI at 7T using radial-Cartesian TURBINE sampling. Magn Reson Med 2022;88(5): 2058-2073.
- Raimondo L, Knapen T, Oliveira MAF, et al. A line through the brain: Implementation of human line-scanning at 7T for ultra-high spatiotemporal resolution fMRI. J Cereb Blood Flow Metab 2021;41(11):2831-2843.
- 47. Huber L, Finn ES, Chai Y, et al. Layer-dependent functional connectivity methods. Prog Neurobiol 2021;207:101835.
- Guidi M, Huber L, Lampe L, Merola A, Ihle K, Möller HE. Cortical laminar resting-state signal fluctuations scale with the hypercapnic blood oxygenation level-dependent response. Hum Brain Mapp 2020;41(8): 2014-2027.
- Mansfield P. Multi-planar image formation using NMR spin echoes. J Phy C: Solid State Phys 1977;10(3):L55-L58.
- Havlicek M, Uludağ K. A dynamical model of the laminar BOLD response. Neuroimage 2020;204:116209.

- Carr HY. Steady-state free precession in nuclear magnetic resonance. Phys Rev 1958;112:1693-1701.
- Yacoub E, Van De Moortele PF, Shmuel A, Uğurbil K. Signal and noise characteristics of Hahn SE and GE BOLD fMRI at 7 T in humans. Neuroimage 2005;24(3):738-750.
- Günther M, Oshio K, Feinberg DA. Single-shot 3D imaging techniques improve arterial spin labeling perfusion measurements. Magn Reson Med 2005;54(2):491-498.
- Hua J, Qin Q, van Zijl PC, Pekar JJ, Jones CK. Whole-brain threedimensional T2-weighted BOLD functional magnetic resonance imaging at 7 Tesla. Magn Reson Med 2014;72(6):1530-1540.
- Scheffler K, Ehses P. High-resolution mapping of neuronal activation with balanced SSFP at 9.4 Tesla. Magn Reson Med 2016;76(1): 163-171.
- Margosian P, Faster MR. Imaing Imaging with half the data. Proceedings of the 4th Annual Meeting of SMRM. International Society for Magnetic Resonance in Medicine, London; 1985. p 1024.
- Chapman B, Turner R, Ordidge RJ, et al. Real-time movie imaging from a single cardiac cycle by NMR. Magn Reson Med 1987;5: 246-254.
- Zaitsev M, Zilles K, Shah NJ. Shared k-space echo planar imaging with keyhole. Magn Reson Med 2001;45(1):109-117.
- Shah NJ, Zilles K. Verfahren zur Untersuchung eines Objektes mittels Erfassung des Ortsfrequenzraumes. German Patent Application. 2003; No. 199 62 845 C2.
- Shah NJ, Zilles K. Imaging process in the spatial frequency space and useful for examining the properties of object. USA Patent Application. 2004; No. 6781372 B2.
- Yun SD, Reske M, Vahedipour K, Warbrick T, Shah NJ. Parallel imaging acceleration of EPIK for reduced image distortions in fMRI. Neuroimage 2013;73:135-143.
- Yun SD, Shah NJ. Whole-brain high in-plane resolution fMRI using accelerated EPIK for enhanced characterisation of functional areas at 3T. PloS One 2017;12(9):e0184759.
- Yun SD, Weidner R, Weiss PH, Shah NJ. Evaluating the utility of EPIK in a finger tapping fMRI experiment using BOLD detection and effective connectivity. Sci Rep 2019;9(1):10978.
- 64. Küppers F, Yun SD, Shah NJ. Development of a novel 10-echo multicontrast sequence based on EPIK to deliver simultaneous quantification of T2 and T2\* with application to oxygen extraction fraction. Magn Reson Med 2022;88(4):1608-1623.
- Yun SD, Shah NJ. Analysis of EPI phase correction with low flip-angle excitation to reduce the required minimum TE: Application to wholebrain, submillimeter-resolution fMRI at 3 T. Magn Reson Med 2020; 84(3):1416-1429.
- 66. Yun SD, Shah NJ. An evaluation of high-resolution EPI sequences and enhanced image reconstruction for fMRI at 7T: Siemens-EPI, CMRR-EPI and INM4-EPI. Proceedings of the 31st Annual Meeting of ISMRM. International Society for Magnetic Resonance in Medicine, London; 2022. (abstract 3281).
- 67. Feinberg DA, Harel N, Ramanna S, Ugurbil K, Yacoub E. Sub-millimeter single-shot 3D GRASE with inner volume selection for T2 weighted fMRI applications at 7 Tesla. *Proceedings of the 16th Annual Meeting of ISMRM*. International Society for Magnetic Resonance in Medicine, Toronto; 2008. (abstract 2373).
- Kemper VG, De Martino F, Yacoub E, Goebel R. Variable flip angle 3D-GRASE for high resolution fMRI at 7 Tesla. Magn Reson Med 2016;76(3):897-904.
- Narsude M, Gallichan D, van der Zwaag W, Gruetter R, Marques JP. Three-dimensional echo planar imaging with controlled aliasing: A sequence for high temporal resolution functional MRI. Magn Reson Med 2016;75(6):2350-2361.
- Poser BA, Koopmans PJ, Witzel T, Wald LL, Barth M. Three dimensional echo-planar imaging at 7 Tesla. Neuroimage 2010;51(1): 261-266.

- Jorge J, Figueiredo P, van der Zwaag W, Marques JP. Signal fluctuations in fMRI data acquired with 2D-EPI and 3D-EPI at 7 Tesla. Magn Reson Imaging 2013;31(2):212-220.
- Reynaud O, Jorge J, Gruetter R, Marques JP, van der Zwaag W. Influence of physiological noise on accelerated 2D and 3D resting state functional MRI data at 7 T. Magn Reson Med 2017;78(3):888-896.
- 73. Triantafyllou C, Hoge RD, Krueger G, et al. Comparison of physiological noise at 1.5 T, 3 T and 7 T and optimization of fMRI acquisition parameters. Neuroimage 2005;26(1):243-250.
- Stöcker T, Kellermann T, Schneider F, et al. Dependence of amygdala activation on echo time: Results from olfactory fMRI experiments. Neuroimage 2006;30(1):151-159.
- Posse S, Wiese S, Gembris D, et al. Enhancement of BOLD-contrast sensitivity by single-shot multi-echo functional MR imaging. Magn Reson Med 1999;42(1):87-97.
- Kundu P, Voon V, Balchandani P, Lombardo MV, Poser BA, Bandettini PA. Multi-echo fMRI: A review of applications in fMRI denoising and analysis of BOLD signals. Neuroimage 2017;154:59-80.
- Puckett AM, Bollmann S, Poser BA, Palmer J, Barth M, Cunnington R. Using multi-echo simultaneous multi-slice (SMS) EPI to improve functional MRI of the subcortical nuclei of the basal ganglia at ultra-high field (7T). Neuroimage 2018;172:886-895.
- Yun S, Oh SS, Han Y, Park H. High-resolution fMRI with higher-order generalized series imaging and parallel imaging techniques (HGS-parallel). J Magn Reson Imaging 2009;29(4):924-936.
- Báez-Yánez MG, Ehses P, Mirkes C, Tsai PS, Kleinfeld D, Scheffler K. The impact of vessel size, orientation and intravascular contribution on the neurovascular fingerprint of BOLD bSSFP fMRI. Neuroimage 2017;163:13-23.
- Kasper L, Engel M, Heinzle J, et al. Advances in spiral fMRI: A highresolution study with single-shot acquisition. Neuroimage 2022;246: 118738
- Zaitsev M, Maclaren J, Herbst M. Motion artifacts in MRI: A complex problem with many partial solutions. J Magn Reson Imaging 2015; 42(4):887-901. https://doi.org/10.1002/jmri.24850.
- Fang Z, Van Le N, Choy M, Lee JH. High spatial resolution compressed sensing (HSPARSE) functional MRI. Magn Reson Med 2016; 76(2):440-455.
- Jiang W, Larson PEZ, Lustig M. Simultaneous auto-calibration and gradient delays estimation (SAGE) in non-Cartesian parallel MRI using low-rank constraints. Magn Reson Med 2018;80(5):2006-2016.
- Donoho DL. Compressed sensing. IEEE Trans Inf Theory 2006;52(4): 1289-1306
- Zong X, Lee J, John Poplawsky A, Kim SG, Ye JC. Compressed sensing fMRI using gradient-recalled echo and EPI sequences. Neuroimage 2014;92:312-321.
- Heiler PM, Konstandin S, Schad LR. Inner volume BOLD-fMRI at ultrahigh spatial resolution. *Proceedings of the 17th Annual Meeting of ISMRM*. International Society for Magnetic Resonance in Medicine, Honolulu; 2009. (abstract 1551).
- Zhao L, Madore B, Panych LP. Reduced field-of-view MRI with twodimensional spatially-selective RF excitation and UNFOLD. Magn Reson Med 2005;53(5):1118-1125.
- Katscher U, Börnert P, Leussler C, van den Brink JS. Transmit SENSE. Magn Reson Med 2003;49(1):144-150.
- Wilm BJ, Svensson J, Henning A, Pruessmann KP, Boesiger P, Kollias SS. Reduced field-of-view MRI using outer volume suppression for spinal cord diffusion imaging. Magn Reson Med 2007;57(3): 625-630.

- Heidemann RM, Ivanov D, Trampel R, et al. Isotropic submillimeter fMRI in the human brain at 7 T: Combining reduced field-of-view imaging and partially parallel acquisitions. Magn Reson Med 2012; 68(5):1506-1516.
- Zaitsev M, Hennig J, Speck O. Point spread function mapping with parallel imaging techniques and high acceleration factors: Fast, robust, and flexible method for echo-planar imaging distortion correction. Magn Reson Med 2004;52(5):1156-1166.
- Bowtell R, McIntyre DJO, Commandre MJ, Glover PM, Mansfield P. Correction of geometric distortion in echo planar images. Proceedings of the 2nd Annual Meeting of SMR.International Society for Magnetic Resonance in Medicine, San Francisco; 1994. p 411.
- 93. Yun SD, Erhan G, Shah NJ. A simultaneous measurement of opposite-phase-encoding EPI in a single fMRI session for the reduction of acquisition time and SAR at 7T. *Proceedings of the 32nd Annual Meeting of ISMRM*. International Society for Magnetic Resonance in Medicine, Toronto; 2023. (abstract 1161).
- Polimeni JR, Renvall V, Zaretskaya N, Fischl B. Analysis strategies for high-resolution UHF-fMRI data. Neuroimage 2018;168:296-320.
- van der Zwaag W, Buur PF, Fracasso A, et al. Distortion-matched T1 maps and unbiased T1-weighted images as anatomical reference for high-resolution fMRI. Neuroimage 2018;176:41-55.
- 96. Menon RS. Postacquisition suppression of large-vessel BOLD signals in high-resolution fMRI. Magn Reson Med 2002;47(1):1-9.
- Raimondo L, Oliveira MAF, Heij J, et al. Advances in resting state fMRI acquisitions for functional connectomics. Neuroimage 2021;243: 118503.
- Gao JH, Liu HL. Inflow effects on functional MRI. Neuroimage 2012; 62(2):1035-1039.
- Pais-Roldán P, Yun SD, Shah NJ. Pre-processing of sub-millimeter GE-BOLD fMRI data for laminar applications. Front Neuroimaging 2022;1: 869454
- Vazquez AL, Fukuda M, Crowley JC, Kim SG. Neural and hemodynamic responses elicited by forelimb- and photo-stimulation in channelrhodopsin-2 mice: Insights into the hemodynamic point spread function. Cereb Cortex 2014;24(11):2908-2919.
- Chaimow D, Yacoub E, Uğurbil K, Shmuel A. Spatial specificity of the functional MRI blood oxygenation response relative to neuronal activity. Neuroimage 2018;164:32-47.
- 102. Yun SD, Shah NJ. The spatial resolution of partial-Fourier-accelerated EPI to delineate a submillimetre voxel at 7T: Use of an intensive partial Fourier factor. Proceedings of the 31st Annual Meeting of ISMRM. International Society for Magnetic Resonance in Medicine, London; 2022. (abstract 3899).
- Teves JB, Gonzalez-Castillo J, Holness M, Spurney M, Bandettini PA, Handwerker DA. The art and science of using quality control to understand and improve fMRI data. Front Neurosci 2023;17:1100544. https://doi.org/10.3389/fnins.2023.1100544.
- 104. Sharoh D, van Mourik T, Bains LJ, et al. Laminar specific fMRI reveals directed interactions in distributed networks during language processing. Proc Natl Acad Sci U S A 2019;116(42):21185-21190. https://doi.org/10.1073/pnas.1907858116.
- Power JD, Mitra A, Laumann TO, Snyder AZ, Schlaggar BL, Petersen SE. Methods to detect, characterize, and remove motion artifact in resting state fMRI. Neuroimage 2014;84:320-341. https://doi.org/10.1016/j.neuroimage.2013.08.048.
- Miller KL, Bartsch AJ, Smith SM. Simultaneous multi-slice imaging for resting-state fMRI. MAGNETOM Flash 2015;63:70-77.